



THESIS

2

MICHIGAN STATE UNIVERSITY LIBRARIES



3 1293 01417 2708

This is to certify that the

dissertation entitled

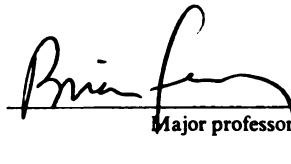
A METHOD OF PARAMETRIC IDENTIFICATION
FOR CHAOTIC SYSTEMS

presented by

Ching-Ming Yuan

has been accepted towards fulfillment
of the requirements for

Ph.D. degree in Mechanical Engineering


Major professor

Date 19 May 95

**LIBRARY
Michigan State
University**

**PLACE IN RETURN BOX to remove this checkout from your record.
TO AVOID FINES return on or before date due.**

DATE DUE	DATE DUE	DATE DUE
_____	_____	_____
_____	_____	_____
_____	_____	_____
_____	_____	_____
_____	_____	_____
_____	_____	_____
_____	_____	_____

**A METHOD OF
PARAMETRIC IDENTIFICATION FOR
CHAOTIC SYSTEMS**

By

Ching-Ming Yuan

A DISSERTATION

**Submitted to
Michigan State University
in partial fulfillment of the requirements
for the degree of**

DOCTOR OF PHILOSOPHY

Department of Mechanical Engineering

1995

ABSTRACT

A METHOD OF PARAMETRIC IDENTIFICATION FOR CHAOTIC SYSTEMS

By

Ching-Ming Yuan

A method for identifying parameters in a mathematical model of a chaotic system is presented. It is an extension of an existing method for nonlinear systems with stable periodic response. The method exploits the chaotic attractor, and extracts the unstable periodic orbits from the attractor to represent the system behavior. Each term in the mathematical model is expressed in a finite Fourier series using the extracted periodic-orbits, and the harmonic-balance method is applied to form a set of linear algebraic equations in system parameters for least-squares estimation.

This method has been successfully applied numerically to a forced Duffing oscillator, a smooth Coulomb friction system, a parametrically forced system, and a Lorenz oscillator, and experimentally to a forced oscillator with a two-well stiffness potential.

The identified models have been verified by comparing the Lyapunov exponents, the structure of the unstable periodic orbits, and the bifurcation diagrams of the original system and the identified model.

To my parents

ACKNOWLEDGEMENTS

I am very grateful to my thesis chairman and advisor, Professor Brian Feeny, for his introduction to chaotic systems, for his understanding of my poor English, and his encouragement and guidance in the research. His promptness and attention to detail were extremely helpful. I thank Professor Alan Haddow for his excellent teaching in nonlinear mechanical vibrations, for his friendship, and for helping my family in adjusting to a foreign environment. I thank Professor Hassan Khalil, who also provided excellent teaching in linear and nonlinear control theory, and stimulated ideas in my research. I also thank professor Tien-Yien Li for participating in my thesis committee. My warm thanks are also due to Professor David S.-Y. Yen, who left my thesis committee due to a medical leave. I wish him the best for his health.

A special appreciation goes to Professor Joe Cusumano and Bart Kimble at Penn State University for generously giving me the experimental data and detailed explanations of the experiment. Without this, I would probably be working on this research for another year.

A warm thank you goes to my colleague Shyh-Leh Chen, who was always enthusiastic and eager to help in many ways. He provided many critical ideas and suggestions in my thesis. Also, thanks to my other colleagues, Matt Brach, C. P. Chao, J. W. Liang, and Ramana Kappagantu, for good discussions and companionship during my stay in MSU.

Without my parents, I would not be here. My parents have never gone to school--not even a single day in their lives--but have worked very hard to send me and my brothers to school for as high an education as we could attain. They believe that academic achievement is the highlight of the family history. Their spiritual support played a crucial role in the completion of this thesis. I am also indebted to my parents-in-law, who provided extra financial support for my family, subsiding my worries about living in America.

My wife and my two daughters, Ting-fang and Yu-hua, came to this country shortly after me. Ting-fang and Yu-hua came here with no English background, and were my main concern other than my study. They went to Spartan Village Elementary School, with great courage and determination. They slowly but steadily improved their English, made friends and enlarged their knowledge of American culture. Ting-fang went on to Hannah Middle School as a 6th grader and then to MacDonald Middle School as a 7th grader due to the school district reorganization. Yu-hua continued through 4th grade in Spartan Village School. They now enjoy their school lives very much. I am grateful to the faculty and staff of Spartan Village School for providing multi-national cultural environments, and excellent teaching for the international students. The same goes to Hannah Middle School and MacDonald Middle School too.

Of course my wife played an important role regarding life in America. She takes care of our daily lives. She is a very good cook. Without her, living in America would become more difficult and less enjoyable. I deeply appreciated her moral support.

This research was supported financially by a grant from CSIST, Taiwan.

TABLE OF CONTENTS

LIST OF TABLES	ix
LIST OF FIGURES	x
1 Introduction	1
1.1 An Overview of the Parametric Identification Methods	2
1.2 Chaotic Motion	4
1.3 Motivation	7
1.4 Thesis Overview	8
2 Methodology	10
2.1 Introduction	10
2.2 Periodic Orbit Extraction	11
2.3 The Choice of a Mathematical Model	14
2.4 Algorithm	17
2.4.1 Externally Excited Systems	17
2.4.2 Parametrically Excited Systems	21
2.4.3 Autonomous Systems	23
2.5 Strategy for Model Validation	24
2.6 Summary	25
3 Numerical Results	26
3.1 The Forced Duffing Oscillator	27
3.1.1 Extraction of the Periodic Orbits	28
3.1.2 Choosing a Mathematical Model	29
3.1.3 Identification Results	30
3.1.4 Model Verification	31
3.1.5 Effect of Noise	32
3.2 A Smooth Coulomb Friction System	37

3.2.1	Effect of Noise	41
3.3	A Parametrically Excited System	42
3.3.1	Effect of Noise	46
3.4	An Autonomous System: the Lorenz Equations.....	46
3.4.1	Effect of Noise	51
3.5	A Case Study on Modeling the Nonlinearity with a Power Series	52
3.5.1	Using the Known Function in the Model	54
3.5.2	Using the Power Series Approximation	54
3.6	Conclusion	56
4	Experimental Results	58
4.1	Introduction.....	58
4.2	Experimental Setup.....	58
4.3	Phase-Space Reconstruction.....	60
4.4	Periodic-Orbit Extraction	64
4.5	Choosing a Mathematical Model	67
4.6	Data Processing Issues	67
4.7	Identification Results and Model Verification	69
4.8	Estimation of the Natural Frequency and the Damping Ratio	74
4.9	Discussion.....	76
5	Errors in Parameter Estimates	78
5.1	Introduction.....	78
5.2	Errors Induced by Noise.....	79
5.3	Errors Induced by the Periodic Orbit Extraction	81
5.4	Sensitivity of the Parameter Estimates to Errors	86
5.5	Using Several Periodic Orbits.....	88
6	Conclusions and Future Work.....	90
6.1	Conclusions.....	90
6.2	Future Work	93

BIBLIOGRAPHY 95

LIST OF TABLES

Table 1	Identification results using individual periodic orbit for Duffing's equation.....	31
Table 2	Identification results using 4 periodic orbit data for Duffing's equation.....	32
Table 3	Identification results for Duffing's equation using noisy data.....	36
Table 4	Identification results using 4 periodic orbits for Coulomb friction system.....	41
Table 5	Noise effect on identification results for Coulomb friction system.....	42
Table 6	Identification results using 4 periodic orbits for a parametrically excited system	45
Table 7	Noise effect on identification results for a parametrically excited system.....	47
Table 8	Identification results for the Lorenz equation (a).....	51
Table 9	Identification results for Lorenz equation (b).....	52
Table 10	Identification results for Lorenz equation with 1% noise.....	52
Table 11	Force and response in model (3.13).....	53
Table 12	Identification results using the exact function in Model (3.15)	54
Table 13	Identification results using power series in Model (3.16).....	55
Table 14	Identification results for the experimental system.....	69
Table 15	Comparison of the natural frequency and the damping ratio.....	76

LIST OF FIGURES

Figure 2.1	(a) A close recurrence of a chaotic trajectory, and (b) a precise recurrence after a gentle adjustment of the starting point of a chaotic trajectory	12
Figure 3.1	Phase portrait of the Duffing oscillator	28
Figure 3.2	Some extracted periodic orbits of the Duffing oscillator	29
Figure 3.3	The simulated chaotic attractor and some of the extracted periodic orbits of the identified model	33
Figure 3.4	Bifurcation diagrams of the Duffing's equation (a) using the original equation, and (b) using the identified model with the average values in Table 2 .	34
Figure 3.5	(a) A noise-free periodic orbit, (b) the noise-contaminated counterpart . .	35
Figure 3.6	The simulated chaotic attractor and some of the extracted periodic orbits of the identified model using the noise-contaminated periodic orbits	37
Figure 3.7	Bifurcation diagrams of the Duffing's equation (a) using the original equation, (b) using the identified model of the noisy case	38
Figure 3.8	Phase portrait of a Coulomb friction system	39
Figure 3.9	Some extracted periodic orbits of a Coulomb friction system	40
Figure 3.10	Phase portrait of the parametrically excited system	43
Figure 3.11	Some extracted periodic orbits of the parametrically excited system	44
Figure 3.12	Phase portrait of a Lorenz system	48
Figure 3.13	Recurrence plot of the Lorenz system (period lengths are indicated in the numbers of time steps used in the numerical integration)	49
Figure 3.14	Two extracted periodic orbits of a Lorenz system: (a) period length of 110 time steps, (b) period length of 144 time steps	50
Figure 3.15	Nonlinear function in a power series	56
Figure 4.1	Sketch of the experimental setup	59
Figure 4.2	Autocorrelation function of the experimental data	61

Figure 4.3	Correlation function of the experimental data	63
Figure 4.4	Singular system analysis of the experimental data.	64
Figure 4.5	Reconstructed phase space of the experimental system.	65
Figure 4.6	Reconstructed phase space in singular coordinates	65
Figure 4.7	Some extracted periodic orbits from the reconstructed phase space	66
Figure 4.8	Some extracted periodic orbits in singular coordinates	66
Figure 4.9	Qualitative nonlinear function of the experimental system	71
Figure 4.10	Bifurcation diagram of the identified model, (a) with the cubic nonlinear term in the model, and (b) with the fourth power term in the model	72
Figure 4.11	Phase portrait of the identified model with cubic nonlinearity	73
Figure 4.12	Some periodic orbits extracted from the phase portrait of Figure 4.11 . . .	73
Figure 4.13	Transfer function of the right well of the experimental system.	75
Figure 5.1	Close look of the periodic orbit extraction on the Poincare section.	81
Figure 5.2	A sketch of the construction of a linearized map	84

CHAPTER 1

Introduction

Parametric identification deals with the problem of determining the values of the parameters in a mathematical model that represents a dynamical system, based on the observed data from the system. It is a field of increasing interest, in part because of applications in prediction and control.

Linear models have dominated in the description of the dynamical systems and control theoretic approaches. Very complex and randomlike behavior has been viewed from a statistical perspective in which many degrees of freedom were involved. More recently nonlinear models have emerged, capable of describing chaotic dynamics and other nonlinear behaviors. Such systems can exhibit extremely complex dynamical behavior, even though the underlying dynamics may be low dimensional. On the other hand, high-dimensional systems such as fluids and lasers can show simple and low-dimensional dynamics, which may be described by a low dimensional model [43].

Chaotic motion features the sensitive dependence on initial conditions. Nearby orbits that cannot be distinguished will diverge exponentially and soon become uncorrelated. Along with new theoretical concepts have come practical techniques, such as Lyapunov

exponents and fractal dimension, for characterizing the dynamics of such systems. Yet, the techniques for identifying the parameters of a chaotic system are not as well developed as those for analyzing its dynamical behaviors. We briefly review parametric identification methods below.

1.1 An Overview of the Parametric Identification Methods

Parametric identification work generally presupposes that a mathematical model has been chosen to represent a nonlinear system and that the goal is to identify the unknown parameters in the given model. The unknown parameters are determined by optimizing in some sense the fit of the chosen model to the available data.

For linear systems, the superposition principle can be applied to the system response and the transfer function that characterizes the system behavior can be obtained by a variety of techniques, such as transient analysis, frequency analysis, correlation analysis, and spectral analysis [37]. The system parameters are estimated by a curve fitting of the transfer function.

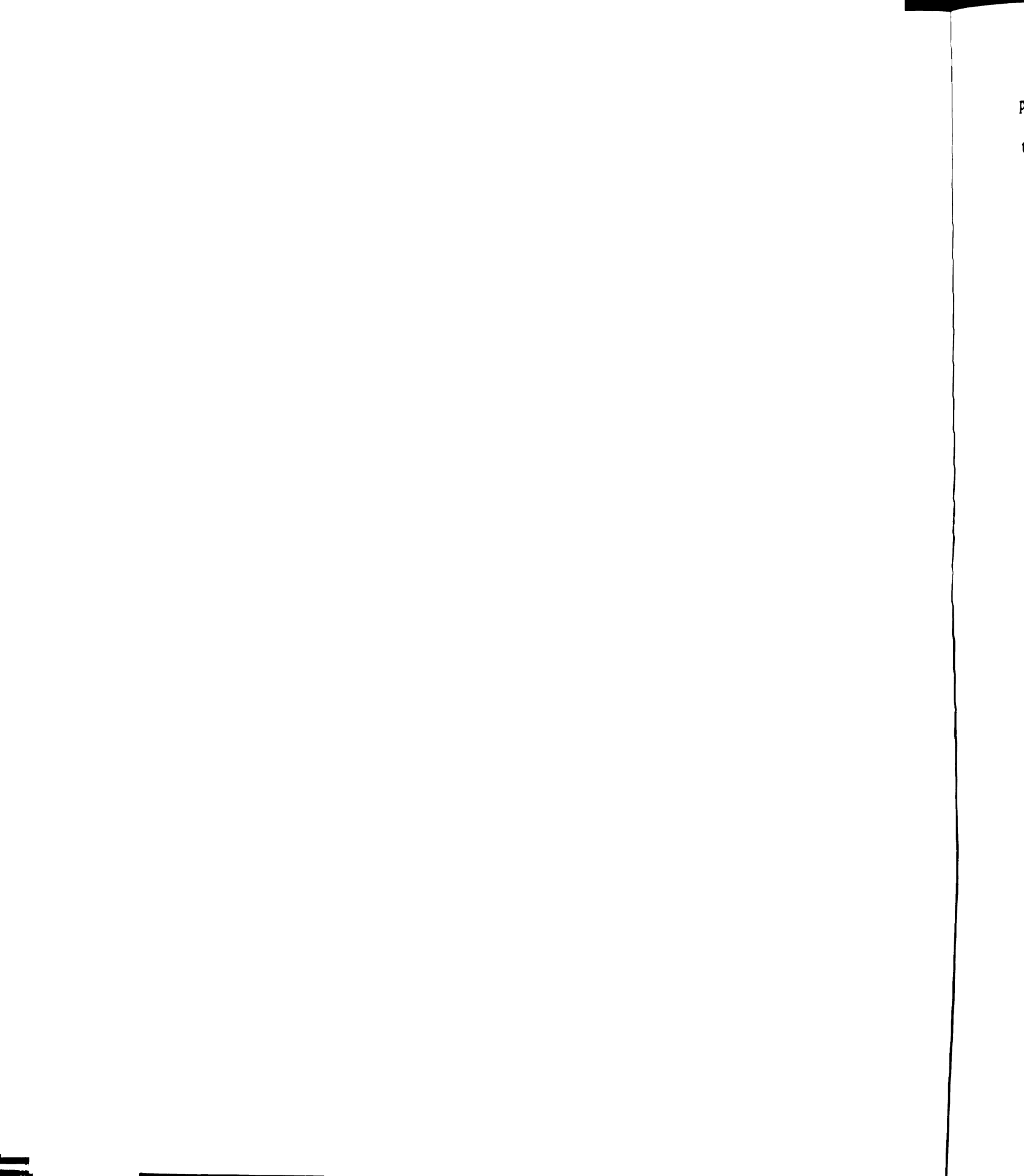
For a nonlinear system, the techniques for linear systems fail fundamentally because the superposition principle is no longer applicable. However, for small nonlinearities, perturbation techniques were widely used in analyzing the system response and in identifying the system parameters as well. For example, Hanagud *et al.* [32] used the method of multiple scales to determine the nominal system response, which was used iteratively to estimate parameters. Nayfeh [45] and Feeny *et al.* [23] used the method of multiple scales to exploit resonances and produce expressions relating the parameters to the experimentally measured nonlinear behavior such as jump phenomena and nonlinear drift. The parameters could then be determined algebraically, or in a least-squares sense.

Ibanez [33] used a describing function method to construct an approximate transfer function of the nonlinear structural system and hence uncouple the original nonlinear equations. System parameters were obtained by iteratively minimizing the error function between the measured data and the theoretical solution. Gottlieb et al. [27] used the Hilbert Transform in their parametric identification of weakly nonlinear systems.

Another approach proposed by Mook *et al.* [41, 42, 52], called the method of minimum model error (MME), combined the assumed model with the measurements to determine the correct form of model for the nonlinear system under investigation. A correction term which represented the model error was added to the assumed model and a cost function was formed. By minimizing the cost function, a two-point-boundary-value problem was formed and yielded the correction term, which was then fitted to an assumed polynomial form to obtain the correct model of the nonlinear system.

Mohammad [40] used a direct approach by assuming a general form of the equation to represent the nonlinear system under investigation. By measuring all of the system responses, such as acceleration, velocity, and position, and directly introducing them into the assumed equation, a set of algebraic equations was formed by balancing these measurements and the input function. System parameters were then estimated by a singular-value decomposition method.

In a similar direct approach, Yasuda *et al.* [59, 60, 61] represented the system nonlinearity as a sum of polynomials in the system equation, with unknown coefficients as the system parameters to be determined. Periodic responses under periodic excitation were measured and expressed in Fourier series. The harmonic balance method was used to balance the Fourier coefficients of each harmonic and a set of algebraic equations in the system



parameters was formed. The system parameters were then estimated by a least squares fit to the algebraic equations.

Recently, methods for modelling a chaotic system and identifying the system parameters based on experimental data have been developed. Abarbanel *et al.* [1] proposed a method for constructing a parameterized map which evolved points in the phase space into the future. This map was regarded as a dynamic system, and the parameter values were chosen through a least-squares optimization procedure, constrained by the invariants of the system, such as the Lyapunov exponents. Eisenhammer *et al.* [20] proposed a *trajectory method* to extract ordinary differential equations from an experimental time series. The experimental data were represented in a state space and the corresponding flow vectors were approximated by polynomials of the state vector components. Starting from appropriately chosen initial states, the model equation was used to obtain an estimation of the states for later times, and the coefficients were fitted by minimizing the distances between the states predicted by the model and the experimental states. Breeden and Hubler [6] proposed a *flow method* for reconstructing a set of coupled maps or ordinary differential equations from a trajectory of the system in state space. By choosing some trial coefficients for a series expansion in the state variable, the error in these parameters were computed by comparing the predicted values and the experimental values. The parameters of the model were obtained by solving a chi-squared minimization problem.

1.2 Chaotic Motion

Chaos was known by Henri Poincare (1854-1912) about a century ago in the course of his investigations on the three-body problem. Through his discovery of homoclinic solutions (homoclinic intersection, or homoclinic tangles), Poincare showed that the three-body

problem has no solutions of the type envisioned by Jacobi or Hamilton, in the sense that a small error in the initial conditions produced an enormous error in the final response. In his book, *New Methods of Celestial Mechanics*, Poincare wrote¹:

When we try to represent the figure formed by these two curves and their intersections in a finite number, each of which corresponds to a doubly asymptotic solution, these intersections form a type of trellis, tissue, or grid with infinitely serrated mesh. Neither of the two curves must ever cut across itself again, but it must bend back upon itself in a very complex manner in order to cut across all of the meshes in the grid an infinite number of times.

The complexity of this figure will be striking, and I shall not even try to draw it. Nothing is more suitable for providing us with an idea of the complex nature of the three-body problem, and of all the problems of dynamics in general, where there is no uniform integral and where the Bohlin series are divergent.

In the words of modern dynamical systems theory, the solution is sensitive to initial conditions due to the inherent stretching and folding process of the nonlinear dynamics. This sensitivity to initial conditions makes the nearby states on the attractor divergent exponentially on the average, and results in a long-term unpredictability emanating from a small amount of uncertainty in the initial conditions.

Confronted with his discovery of the homoclinic solution, Poincare went on inventing several theories for new branches of mathematics, including topology, ergodic theory, homology theory, and the qualitative theory of differential equations. He also pointed out the possible uses of periodic orbits in characterizing his discovery²:

1. See Tufillaro, Abbott, and Reilly in *An Experimental approach to Nonlinear Dynamics and Chaos*, 1992, for more historical comments [53].

... there is a zero probability for the initial conditions of the motion to be precisely those corresponding to a periodic solution. However, it can happen that they differ very little from them, and this takes place precisely in the case where the old methods are no longer applicable. We can then advantageously take the periodic solution as first approximation, as intermediate orbit, to use Gylden's language... Given equations of the form defined in art. 13 and any particular solution of these equations, we can always find a periodic solution (whose period, it is true, is very long), such that the difference between the two solutions is as small as we wish, during as long a time as we wish. In addition, these periodic solutions are so valuable for us because they are, so to say, the only breach by which we may attempt to enter an area heretofore deemed inaccessible.

The periodic orbits are dense in the chaotic attractor, and all of them are unstable. This is a characteristic sign of chaos that only the presence of unstable periodic orbits but absence of the stable ones [2]. The periodic orbit theme has been pursued by many authors in modern dynamical system theory in characterizing a chaotic attractor [5, 19, 35, 49, 53], and in the course of controlling a chaotic system [16, 47, 50]. The unstable periodic orbits have also been used in system identification [31], and in recognizing parameter variations [35]. We use them as a major tool in our parametric identification scheme for a chaotic system.

Chaotic signals have been discarded in the past as 'noise'. But, as pointed out by Abarbanel [2], *'chaos is not an aspect of physical systems which is to be located and discarded, but is an attribute of physical behavior which is quite common and whose*

2. MacKay, R. and Meiss, J., eds., *Hamiltonian dynamical systems* (Adam Hilger, Philadelphia, 1987), cited from Tufillaro, Abbott, and Reilly in *An Experimental approach to Nonlinear Dynamics and Chaos*, 1992 [53]

utilization for science and technology is just beginning'. It has been discovered in many nonlinear systems in the laboratory and in the mathematical models in the past two decades, and has become a well-known phenomenon and an important subject in modern dynamical system theory. Much of the work has concentrated on learning how to classify the nonlinear systems by analyzing the output from known systems. These efforts have provided, and continue to provide, significant insights into the kinds of behavior which one might expect from nonlinear dynamical systems, and have led to an ability to evaluate now familiar quantities such as fractal dimension, Lyapunov exponents, and other invariants of the nonlinear systems [2]. Efforts have also been extended to predicting and controlling the chaotic behaviors. For example, Farmer and Sidorowich [20] proposed a local approximation approach for predicting a short-term chaotic time series using the nearby states. Ott *et al.* [47], Ditto *et al.* [16], and Shinbrot *et al.* [50] tried to control the chaos by exploiting the periodic orbits embedded in a chaotic attractor and perturbing some parameters of the system, so as to stabilize one of the unstable periodic orbits, making the system become stable and more flexible under different operating conditions. Cusumano and Sharkady [12] experimentally studied the bifurcation and dimensionality of a chaotic attractor occurred in a low dimensional parametric-excited system, and built a valid model for the physical system. This trend of study shows that the chaotic motion may be often regarded as an annoyance, yet it provides an extremely useful capability without counterpart in non-chaotic systems.

1.3 Motivation

Chaos is inherent to nonlinear dynamical systems, and is rich in information content as compared to a periodic trajectory. This richness has been exploited in dimensionality

studies, nonlinear prediction, and control schemes as stated in the previous section. The potential usage of chaotic system in parametric identification has not been fully exploited, because of the sensitive dependence on initial conditions and the long-term unpredictability.

It is well known that a chaotic attractor is the closure of the set of unstable periodic orbits [5]. They can be extracted and used to characterize the chaotic attractor [5, 19, 35, 49, 53], and hence can be used for identifying the system parameters, because they are the solution to the system equation.

Meanwhile, Yasuda and co-workers [59, 60, 61] have demonstrated that the stable periodic solution to a nonlinear system can be used to identify the system parameters. This inspires us to explore the applicability of the unstable periodic orbits in a parametric identification scheme for a chaotic system.

1.4 Thesis Overview

In Chapter Two, we describe the methodology for identifying the parameters of a chaotic system. A mathematical model is chosen to fit the characteristic of the original system from which the chaotic data are obtained. The unstable periodic orbits are extracted from a chaotic set for use in the identification algorithm. Then the harmonic-balance method is applied to form a set of linear algebraic equations in system parameters, which are then solved by a least-squares fit. This approach is applied to different kinds of nonlinear systems, such as externally excited, parametrically excited, and autonomous systems.

Chapter Three contains the identification results for several numerical examples. Chaotic data are generated numerically from known governing equations. Mathematical models are chosen in polynomial form generally if no knowledge about the system nonlinearity is

available. Random noise is added to the periodic data to assess its effects on the identification results. The identified models are verified by comparing the Lyapunov exponents, the structure of the unstable periodic orbits, and the bifurcation diagrams of the original system and the identified one.

In Chapter Four, we apply the method to a set of experimental data, taken from J. P. Cusumano and B. W. Kimble at Pennsylvania State University. The phase space is reconstructed by the method of delays, from which the unstable periodic orbits are extracted for use in the identification procedure. A model is obtained and verified for the experimental system.

Two sources of error, noise and the extraction of the periodic orbits, in the identification process are discussed in Chapter Five. We examine a bound on the error in the Fourier coefficients induced by the noise. We examine the extraction of the unstable periodic orbits closely, and establish a bound on the deviation of the extracted periodic orbit from the real one. We discuss the sensitivity of the errors induced by the noise and the extraction of the unstable periodic orbit to the identification results.

Chapter Six contains some conclusions and future work.

CHAPTER 2

Methodology

2.1 Introduction

Parametric identification method is not well developed for a chaotic system, partly because in the past chaos has been treated as noise to be discarded, and partly because chaotic motion exhibits sensitive dependence on initial conditions and defies long-term predictability. Traditional usage of time series data in a parametric identification scheme for non-chaotic systems may not be appropriate for chaotic systems, because of sensitivity to initial conditions. However, a chaotic system features a chaotic attractor¹, in which infinitely many unstable periodic orbits are present, but absent of stable ones [2]. These unstable periodic orbits can be extracted and used to characterize the chaotic attractor [5, 35]. They provide a skeleton of the chaotic set, which can be used in characterizing a chaotic system.

Each unstable periodic orbit is a “solution” to the system which generated the chaotic set. Once a periodic orbit is extracted, each term in the mathematical model can be expressed in a Fourier series, and the harmonic-balance method can be applied to form a set of

1. An attractor is an attracting set which contains a dense orbit. It is difficult to show in examples that a dense orbit exists, and in fact many of the numerically observed “attractors” may not be true attractors but merely attracting sets. We use this term loosely to denote a set of points in phase space toward which a time history approaches after transients die out. See Guckenheimer and Holmes [30] and Moon [43] for strict mathematical definition and examples.

algebraic equations, in which the system parameters are estimated by a least-squares method.

The harmonic-balance method has also been used as a parametric identification technique by Yasuda and coworkers [59, 60, 61] for some nonlinear systems that have stable periodic response. We extend this technique to chaotic systems, where unstable periodic orbits are abundant in the chaotic attractor.

In this chapter, we will demonstrate the methodology in detail with three kinds of chaotic systems, categorized as externally excited, parametrically excited, and autonomous. They are treated differently because the excitation can affect the formulation of the identification problem. We will discuss two important issues to our identification method, the extraction of the unstable periodic orbits and the choice of a valid mathematical model. We will also discuss the method for model verification.

2.2 Periodic Orbit Extraction

The genesis of a chaotic trajectory can be visualized as a random walk on the union of infinitely many periodic orbits [14]. A physical trajectory approaches the saddle orbit along its stable manifold, and remains nearby for a time before it is thrown out along the unstable direction. It wanders around the union of periodic orbits, tracing out a strange¹ attractor [14].

When the trajectory is near a periodic orbit, it approximately follows the motion of that periodic orbit for an interval of time. If this time interval exceeds the period of the reference orbit, the trajectory exhibits a recurrence. This property can be used to

1. The term *strange attractor*, referring to the attractor in the phase space on which chaotic orbits move, is associated with a geometric object called a fractal set, while a *chaotic attractor*, denoting a bounded motion that is sensitive to changes in initial conditions, has at least one positive Lyapunov exponent [43]. In our specific purpose, we intend not to distinguish the difference, but use them interchangeably to refer to the long-term behavior of the nonlinear system.

approximate the positions of the unstable periodic orbits embedded within the attractor [5, 35].

Figure 2.1 is a sketch of a recurrent three-dimensional flow in the vicinity of a hyperbolic periodic orbit [53]. The chaotic trajectory has a recurrent segment, shown in Figure 2.1(a), which is very close to an unstable periodic orbit, shown in Figure 2.1(b). We can gently adjust the “starting point” of the trajectory segment so that the segment nearly coincides with the unstable periodic orbit and returns almost precisely to its starting point [14, 53]. This idea has been used in a control scheme to stabilize one of the unstable periodic orbits for a chaotic system [16, 47, 50].

In practice, we may have a sufficiently large chaotic data set $\{x_i\}$, $i = 1, \dots, N$, in state space. We scan the data set for recurrences by seeking points that come within a specified spatial distance ε of one another after a fixed elapsed time, such that [5, 35]

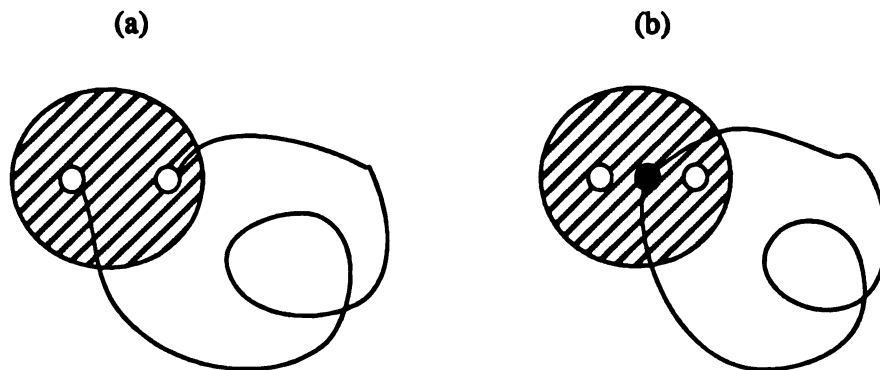


Figure 2.1: (a) A close recurrence of a chaotic trajectory, and (b) a precise recurrence after a gentle adjustment of the starting point of a chaotic trajectory.

$$\|x_{i+K} - x_i\| \leq \varepsilon, \quad (2.1)$$

where K is the number of points per period of the unstable periodic orbit. If x_i is a recurrent point, then x_{i+1}, x_{i+2}, \dots , are likely to be “near” the unstable periodic orbit.

Thus, the segment of data, $\{x_i, x_{i+1}, \dots, x_{i+K-1}\}$, is then taken as the ‘approximated’ unstable periodic orbit. The ‘true’ one is generally unobtainable. The value i is the starting point of the unstable periodic orbit, and is related to the phase angle associated with that periodic orbit relative to the forcing function. It is important to record the phase angle for later use in the calculation of the Fourier coefficients. This will become clear when we do the calculation.

In a periodically forced system, all periodic orbits have a period that is an integer multiple of the forcing period such that $K = n_0, 2n_0, 3n_0, \dots$, where n_0 is the number of points per forcing period [30]. However, in an autonomous system, such as in the Lorenz oscillator, there is no such forcing period. Instead there are infinitely many unstable periodic orbits with incommensurate periods. These incommensurate periods can be obtained using a recurrence plot, which can be constructed by varying the period length and counting the number of recurrent points found for each period length. The recurrence periods will be clustered around certain values, indicating the periodicity of the periodic orbits and hence the number of points in a period, which is then used as the fixed elapsed time K in Eq. (2.1) for locating the periodic orbits, and also used as the fundamental period in the calculation of their Fourier coefficients.

This procedure is quite successful in finding the unstable periodic orbits in many chaotic

systems. However, if the positive Lyapunov exponent associated with the unstable orbit is large, then in one period the orbit will most likely have so departed from the unstable periodic structure in phase space that one will probably not be able to identify the unstable periodic orbit within the spatial criterion. In such case, the spatial distance criterion ϵ can then be relaxed to include more points in the neighborhood. For finding low-order periodic orbits, say less than ten, it is adequate to set ϵ to be 0.5% of the maximum extent of the chaotic attractor [5, 35].

The searching process for the periodic orbits may reveal several distinct unstable periodic orbits with the same period number. Nonetheless, all extracted periodic orbits can be used in the parametric identification algorithm.

2.3 The Choice of a Mathematical Model

For the task of parametric identification, it is important to choose a valid mathematical model to represent the physical system from which the measurements are taken. To do this, we need to know the order of the system and the form of the system nonlinearity.

For typical mechanical vibratory systems, the system order is twice the number of degrees of freedom. Also, for a nonlinear system to be deterministically chaotic, the system has to be three or more dimensional. For a forced single-degree-of-freedom system, a general mathematical model can be written as

$$m\ddot{x} + f(x, \dot{x}, t) = 0, \quad (2.2)$$

where the time variable is taken as an additional dimension. For an autonomous chaotic system, a general mathematical model can be written as

$$\dot{y} = h(y), \quad (2.3)$$

for $y \in R^n$, $n \geq 3$.

In the forced case, the general function $f(x, \dot{x}, t)$ can take some specific forms when the excitation and the nonlinearity of the system are known. For example, a system is *externally* excited if it is modeled with an inhomogeneous term in the governing equation, and *parametrically* excited if the system differential equations have time-varying coefficients. Also, the form of the system nonlinearity can be determined using the physical law that governs the system dynamics and the background knowledge about the physical system. For example, $\sin(x)$ is usually used to model a pendulum system. A power series can be used to model a system with an unknown smooth nonlinear function. Whenever possible, models based on the physical mechanism should be employed. Thus, for an externally excited single-degree-of-freedom nonlinear system, Eq. (2.2) can be recast more specifically as

$$m\ddot{x} + \sum_{i=1}^p \beta_i f_i(x, \dot{x}) = E(t), \quad (2.4)$$

where $E(t)$ is a known external excitation, $f_i(x, \dot{x})$ are some known functions of x and \dot{x} , p is the number of nonlinear terms in the system model, and m and β_i are the unknown parameters to be determined. For a parametrically excited nonlinear system, Eq. (2.2) can be recast as

$$m\ddot{x} + \sum_{i=1}^r g_i(t) \left\{ \sum_{j=1}^{p_i} \beta_{ij} f_{ij}(x, \dot{x}) \right\} = 0. \quad (2.5)$$

where $g_i(t)$ are the known parametric excitation functions, $f_{ij}(x, \dot{x})$ are some known

functions of x and \dot{x} , r is the number of excitation terms, p_i are the numbers of the nonlinear terms associated with each excitation functions, m and β_{ij} are the unknown parameters to be identified. And for an autonomous system, Eq. (2.3) can be written as

$$\dot{y}_i = \sum_{j=1}^{p_i} \beta_{ij} h_{ij}(y), \quad i = 1, \dots, n, \quad (n \geq 3), \quad (2.6)$$

where $y = [y_1, \dots, y_n]^T$, and $h_{ij}(y)$ are the nonlinear functions of the state variable y , and p_i are the number of terms in each equation of the model.

If the form of the system nonlinearity in Eq. (2.4) and (2.5) is unknown, but can be assumed as a smooth function, and the system is operated in the neighborhood of the equilibrium point, then the unknown function can be approximated by a truncated power series. This is reasonable, because any smooth function can be represented by a power series in some neighborhood of the origin (equilibrium). However, this approximation by a power series may be accompanied by issues such as convergence and optimal truncation. Ideas of convergence and divergence make sense when we consider infinite series. Since we are using a truncated series, these ideas are not critical. If a power series indeed converges to our function to be identified, then it is best to use as many terms as possible without introducing numerical problems associated with large exponents. If the underlying function has a divergent power series in the range of data, then there would be some optimal truncation which is unknown. Thus, an imperfect identification result seems to be the norm.

2.4 Algorithm

2.4.1 Externally Excited Systems

The mathematical model for an externally excited single-degree-of-freedom system is chosen as Eq. (2.4)

$$m\ddot{x} + \sum_{i=1}^p \beta_i f_i(x, \dot{x}) = E(t), \quad (2.7)$$

where the external exciting function, $E(t)$, is considered to be periodic with single frequency ω , such as

$$E(t) = a \cos(\omega t). \quad (2.8)$$

Upon extraction of the periodic orbits from the chaotic attractor, the nonlinear functions become periodic and can be expressed in Fourier series, such as

$$x_p(t) \equiv \frac{a_0}{2} + \sum_{j=1}^n \left\{ a_j \cos\left(\frac{j\omega t}{k}\right) + b_j \sin\left(\frac{j\omega t}{k}\right) \right\} \quad (2.9)$$

$$\dot{x}_p(t) \equiv \sum_{j=1}^n \left(\frac{j\omega}{k}\right) \left\{ b_j \cos\left(\frac{j\omega t}{k}\right) - a_j \sin\left(\frac{j\omega t}{k}\right) \right\} \quad (2.10)$$

$$\ddot{x}_p(t) \equiv - \sum_{j=1}^n \left(\frac{j\omega}{k}\right)^2 \left\{ a_j \cos\left(\frac{j\omega t}{k}\right) + b_j \sin\left(\frac{j\omega t}{k}\right) \right\} \quad (2.11)$$

$$f_i(x, \dot{x})_p \equiv \frac{c_{i0}}{2} + \sum_{j=1}^n \left\{ c_{ij} \cos\left(\frac{j\omega t}{k}\right) + d_{ij} \sin\left(\frac{j\omega t}{k}\right) \right\} \quad (2.12)$$

with the Fourier coefficients calculated as

w

F

c

s

c

e

m

eq

coe

met

balan

In thi

$$\begin{aligned}
 a_j &= \frac{2}{T} \int_{\phi}^{T+\phi} x_p(t) \cos\left(\frac{j\omega t}{k}\right) dt \\
 b_j &= \frac{2}{T} \int_{\phi}^{T+\phi} x_p(t) \sin\left(\frac{j\omega t}{k}\right) dt
 \end{aligned} \tag{2.13}$$

$$\begin{aligned}
 c_{ij} &= \frac{2}{T} \int_{\phi}^{T+\phi} f_i(x, \dot{x})_p \cos\left(\frac{j\omega t}{k}\right) dt \\
 d_{ij} &= \frac{2}{T} \int_{\phi}^{T+\phi} f_i(x, \dot{x})_p \sin\left(\frac{j\omega t}{k}\right) dt
 \end{aligned} \tag{2.14}$$

where the subscript p denotes the function being evaluated using the period- k data, T is the period of the employed periodic orbit, and ϕ is the phase angle of the extracted periodic orbit relative to the forcing. Since the phase angle has been included *implicitly* in the periodic-orbit data and the nonlinear functions (the beginning of the periodic orbit is the index of the phase angle), the limits of integration in Eq. (2.13) and (2.14) are used in the numerical integration of the data. Ignoring the phase angle will cause an inconsistency in the Fourier series representation in Eq. (2.9) to (2.12), and consequently produce incorrect identification results.

Substituting these Fourier series into the model equation (2.7), and balancing the Fourier coefficients of Eq. (2.13) through (2.14) of any set of harmonics, a set of linear algebraic equations in system parameters can be constructed. This usage of the harmonic balance method contrasts its usual usage for response analysis, where the ordinary differential equation is known, and the effort is to solve a set of nonlinear equations in Fourier coefficients. For systems forced with a single harmonic, and for autonomous systems, the method of harmonic balance requires nonlinearity so that several harmonics can be balanced.

In this thesis, we typically use the multiples of the primary harmonic. Thus, for the

exam

or,

wh

coe

con

coe

peri

repr

matri

If $2n$

unique

overdeu

but a be

solution

most con

example of $k = 1$, the balance equations, in matrix form, are

$$\begin{bmatrix} 0 & c_{00} & \dots & c_{p0} \\ -\omega^2 a_1 & c_{11} & \dots & c_{p1} \\ -\omega^2 b_1 & d_{11} & \dots & d_{p1} \\ \dots & \dots & \dots & \dots \\ -(n\omega)^2 a_n & c_{1n} & \dots & c_{pn} \\ -(n\omega)^2 b_n & d_{1n} & \dots & d_{pn} \end{bmatrix} \begin{bmatrix} m \\ \beta_1 \\ \beta_2 \\ \dots \\ \beta_p \end{bmatrix} = \begin{bmatrix} 0 \\ a \\ 0 \\ \dots \\ 0 \\ 0 \end{bmatrix} \quad (2.15)$$

or,

$$A\alpha = q, \quad (2.16)$$

where α is the parameter vector of the system model; A is a $(2n + 1) \times (p + 1)$ coefficient matrix, with each column containing the Fourier coefficients of the corresponding term in the system model; q is a $(p + 1)$ vector, containing the Fourier coefficients of the external forcing function, which contains a non-zero element a in our periodic excitation case; and n is the number of terms retained in the Fourier series representation. For general values of k , the indices and frequencies in the elements of matrix A are scaled by k .

If $2n = p$ and the matrix A is non-singular, the parameter vector α can be determined uniquely. In practice, it is statistically better if the algebraic equation of Eq. (2.16) is overdetermined, so that $2n > p$. Consequently the exact solution will not generally exist, but a best solution can be obtained by a method such as a least-squares fit. We seek a solution that can minimize the average error in all of the equations. The error function is most conveniently chosen as the sum of squares, or defined as [4]

$$e = \|A\alpha - q\|. \quad (2.17)$$

The solution that minimizes Eq. (2.17) is called the least-squares solution of the linear system. The minimization of the error function is performed by setting the partial derivatives of the squared error function with respect to the parameters equal to zero, i.e.

$\partial e^2 / \partial \alpha = 0$, which leads to the so-called *normal equations* as

$$A^T (A\alpha - q) = 0, \quad (2.18)$$

and the least-squares solution of the parameters vector α is

$$\alpha = \left(A^T A \right)^{-1} A^T q. \quad (2.19)$$

Since the operation of a matrix inversion is less accurate and time consuming, the normal equation is often not recommended in the numerical implementation. The most general least-squares solution using the singular-value decomposition method is

$$\alpha = V \Sigma^\dagger U^T q = A^\dagger q, \quad (2.20)$$

where through the singular-value decomposition, $A = U \Sigma V^T$, and A^\dagger is its pseudo-inverse; U and V are the orthogonal matrices with each column consisting of the left and the right singular vectors of matrix A respectively; and Σ^\dagger is the pseudo-inverse of Σ , which has the non-negative diagonal elements being the inverse of that of the corresponding terms in Σ . (See, for examples, Atkinson [4] and Strang [51] for a geometric discussion).

Here arises a question as to how many terms should be retained in the Fourier series representation of a periodic solution. Theoretically, the number of terms in the Fourier series should be infinite, but Mickens [39] has shown that the upper bounds of the absolute

magnitudes of the harmonic coefficients decrease exponentially, such that they become ineffective in the least-squares estimation procedures. We found that the rule of thumb for retaining the number of terms in the Fourier series is

$$3 \leq n \leq 5, \quad (2.21)$$

where n is the number of harmonics of the primary (driving) frequency. This limits the number of unknown parameters in the model that can be estimated using a single periodic orbit. However, we can use several periodic orbits to form several sets of algebraic equations, thereby augmenting the matrix A to increase the redundancy of algebraic equations for the least-squares estimation. This treatment can improve estimation result even if the number of unknown parameters is not excessively large. Moreover, when the parameter set is small, each set of algebraic equations formed by individual periodic orbit can be used separately to obtain statistical information such as mean values and standard deviations. This availability of several extracted periodic orbits from a chaotic set increases the applicability beyond that of a simple periodic response, such as the case by Yasuda and coworkers [59, 60, 61].

2.4.2 Parametrically Excited Systems

A parametrically excited system has time-varying coefficients in the governing equations of motion. Examples of this kind of nonlinear system are a pendulum with a moving support [46], a column with an axial time-varying force [46], and a flexible beam under an electromagnetic force [12]. Previous studies have focused on dynamic stability, in which the introduction of a small vibrational loading can stabilize (destabilize) a system which was statically unstable (stable) [46]. Recent studies show that the system can exhibit

cha

The

cho

This

side

fac

div

app

har

Us

per

con

wit

Her

the

chaotic behavior in a large range of parameters [12, 38].

The mathematical model for a single-degree-of-freedom parametrically excited system is chosen as Eq. (2.5),

$$m\ddot{x} + \sum_{i=1}^r g_i(t) \left\{ \sum_{j=1}^{p_i} \beta_{ij} f_{ij}(x, \dot{x}) \right\} = 0. \quad (2.22)$$

This model is a degenerate case of a parameter estimation problem because the right-hand side of the equation is zero. Also, the Fourier series representations must account for the fact that the system variables are coupled with a time-varying function. To proceed, we divide through by m . The \ddot{x} term is taken as a known quantity by the fact that the approximate periodic solution of the original system is known, and moved to the right-hand side of the equation.

Using the extracted periodic orbits, the evaluated nonlinear functions in the model are periodic. The excitation functions in time and the nonlinear functions in x and \dot{x} are combined together when they are to be expressed in Fourier series, such that

$$\tilde{g}_{ij}(x, \dot{x}, t) = g_i(t) f_{ij}(x, \dot{x}) = \frac{c_{ij0}}{2} + \sum_{k=1}^n c_{ijk} \cos(k\omega t) + d_{ijk} \sin(k\omega t). \quad (2.23)$$

with the Fourier coefficients calculated as

$$\begin{aligned} c_{ijk} &= \frac{2}{T} \int_{\phi}^{T+\phi} \tilde{g}_{ij}(x, \dot{x}, t) \cos(k\omega t) dt \\ d_{ijk} &= \frac{2}{T} \int_{\phi}^{T+\phi} \tilde{g}_{ij}(x, \dot{x}, t) \sin(k\omega t) dt \end{aligned} \quad (2.24)$$

Here, the phase angle is included in the combined nonlinear function $\tilde{g}_{ij}(x, \dot{x}, t)$ through the variable x . The limits of integration are chosen to match with the phase angle of the

ext

Sub

coe

con

2.4

An

fam

The

whi

inco

To e

by c

The

chos

inve

perio

can t

from

phase

extracted periodic orbits.

Substituting the Fourier series into the model equation (2.22), and balancing the Fourier coefficients of each harmonic, a set of algebraic equations such as Eq. (2.16) can be constructed, and the parameters can be estimated by a least-squares fit.

2.4.3 Autonomous Systems

An autonomous system of dimension three or more can exhibit chaotic behavior [30]. The famous example is the Lorenz equation, given by

$$\begin{aligned} \dot{y}_1 &= \sigma(y_2 - y_1) \\ \dot{y}_2 &= \rho y_1 - y_2 - y_1 y_3 \\ \dot{y}_3 &= -\beta y_3 + y_1 y_2 \end{aligned} \tag{2.25}$$

There exists a 'butterfly shaped' chaotic attractor, in some region of the parameter space, which consists densely of infinite many unstable periodic orbits whose periods are incommensurate.

To extract the unstable periodic orbits, the incommensurate periods have to be determined by constructing a recurrence plot, as stated in section 2.2.

The mathematical model for an autonomous system is chosen as Eq. (2.6). It can be chosen more specifically if we know the type of the autonomous system under investigation. In an experiment, each state variable y_i must be measured. Using the periodic orbits extracted from the chaotic attractor, each term in the model is periodic and can be expressed in a Fourier series with the fundamental frequency as the one obtained from the recurrence plot. The Fourier coefficients are calculated as before, except the phase angle can be ignored since there is no forcing function involved. Treating the y_i -

u

e

p

2.

TI

th

as

the

mo

and

con

inv

[11]

[27]

We

data

para

The

tech

know

by W

the ic

We w

terms as known quantities, and balancing the Fourier coefficients of each harmonic in each equation, a set of algebraic equations of the form of Eq. (2.16) is formed. The system parameters are then obtained using a least-squares fit.

2.5 Strategy for Model Validation

The final step, and perhaps the most difficult step, in parametric identification procedure is the model validation. The objectives of validation are to seek answers to questions such as: Is the identified model adequate? Under what conditions is the model representative the system? Traditionally, the method of model validation is to simulate both system and model under similar conditions and compare the respective responses. This is subjective and lacks consistency for chaotic systems, due to the system's sensitivity to the initial conditions [3, 57]. More sophisticated criteria based on geometrical and statistical invariants have been proposed, such as embedding trajectories [9, 43], Poincare sections [11], bifurcation diagrams [3], Lyapunov exponents [1, 58], and the correlation dimension [27], to characterize and compare reconstructed attractor and identified model.

We will seek consistency of the identification results from using different periodic-orbit data sets. This is the most convenient way to check the quality of the identified parameters.

The positive Lyapunov exponent is an invariant quantity of a chaotic system. Several techniques have been developed into algorithm for estimating Lyapunov exponents from a known dynamical system or from observable [5, 19, 35, 58]. We use the computer codes by Wolf *et al.* [58] to calculate the Lyapunov exponents, which will be used in verifying the identified model.

We will also compare the structure of the unstable periodic orbits that are extracted from

the c

reaso

The

chao

The

by A

2.6

We h

unsta

conce

physi

mode

balan

by a l

Meth

This i

period

the me

sensitiv

the original attractor and from the one generated from the identified model. This is reasonable because the unstable periodic orbits are the skeleton of the chaotic attractor. The structure of the periodic orbits would provide some geometric information of the chaotic system that is useful to assess the quality of the identified model.

The criterion of bifurcation diagrams of the system and the identified model, as suggested by Aguirre and Billings [3], will also be used as a supplementary criterion when available.

2.6 Summary

We have outlined a scheme for identifying the parameters of chaotic systems by using the unstable periodic orbits that are extracted from the chaotic attractor. The method is simple conceptually and easy to implement. Models are chosen based on the knowledge of the physical system, or on approximation by a power series. Each term in the mathematical model is expressed in a Fourier series, and the Fourier coefficients of each harmonic are balanced to form a set of algebraic equations in system parameters, which are estimated by a least-squares method.

Methods for model verification are proposed.

This is an extension of an existing method, previously applied to systems with a stable periodic response [59, 60, 61], to chaotic systems. By using the unstable periodic orbits, the method exploits the structure of the chaotic set. Thus, we overcome issues such as sensitivity to initial conditions.

CI

Nu

In th

math

to ex

embe

mode

set of

estim

smoo

In thi

frictio

taken

govern

works

interva

system

CHAPTER 3

Numerical Results

In the previous chapter, we presented an approach for identifying parameters in a mathematical model of a nonlinear system that exhibits chaotic behavior. The strategy is to exploit the chaotic attractor of the system and extract the unstable periodic orbits embedded within it. The extracted periodic orbits are used to express each term in the model in a Fourier series, and their coefficients of each harmonic are balanced to form a set of algebraic equations in system parameters, which are then obtained by a least-square estimation. This approach can be applied to a general class of nonlinear systems with smooth nonlinearity.

In this chapter, numerical studies on the forced Duffing oscillator, a smooth Coulomb friction system, a nonlinear parametrically excited system, and a Lorenz equation, are taken to demonstrate the applicability of this approach. Numerical integration of the governing equations is carried out using a 5th-order Runge-Kutta method on a Sun workstation. Typically, 50000 chaotic data points are generated for with a time step interval of one-100th of the forcing period, or with 0.005 time step size in autonomous systems.

The

It is

me

nor

vib

firs

to

T

P

o

V

c

s

v

3.1 The Forced Duffing Oscillator

The forced Duffing oscillator is given as

$$m\ddot{x} + c\dot{x} + \beta x + \gamma x^3 = a \cos \omega t. \quad (3.1)$$

It is a classic differential equation that has been used to model the nonlinear dynamics of mechanical and electrical systems. With $\beta = 0$, Eq. (3.1) is a model for a circuit with a nonlinear inductor [55, 56], and with $\beta < 0, \gamma > 0$, it is a model for the postbuckling vibrations of an elastic column under compressive loads [44]. It can be written as a set of first-order differential equations

$$\begin{aligned} \dot{x}_1 &= x_2/m \\ \dot{x}_2 &= -cx_2 - \beta x_1 - \gamma x_1^3 + a \cos \omega t \end{aligned} \quad (3.2)$$

to fit the format of the computer integration routine in public libraries such as IMSL.

This equation admits chaotic motions for a large range of parameters. We choose the parameter values as $m = 1$, $c = 0.2$, $\beta = \gamma = 1$, and the forcing term as $a = 27$, and $\omega = 1.33$ [54]. These parameters are to be estimated by the present method.

Using the numerical data generated from the governing equation, a phase portrait is constructed as shown in Figure 3.1. We see that the trajectory wanders around the phase space in the attracting set. Any initial condition within the basin of attraction leads to the same qualitative appearance in the phase space. This is the attracting set from which the unstable periodic orbits are to be extracted.

Also, the Lyapunov exponents, indicating the average exponential rates of divergence or convergence of nearby orbits in phase space, are calculated using the computer code by Wolf *et al.* [58]. They converge to $\lambda_1 = 0.18$, and $\lambda_2 = -0.468$, indicating that the

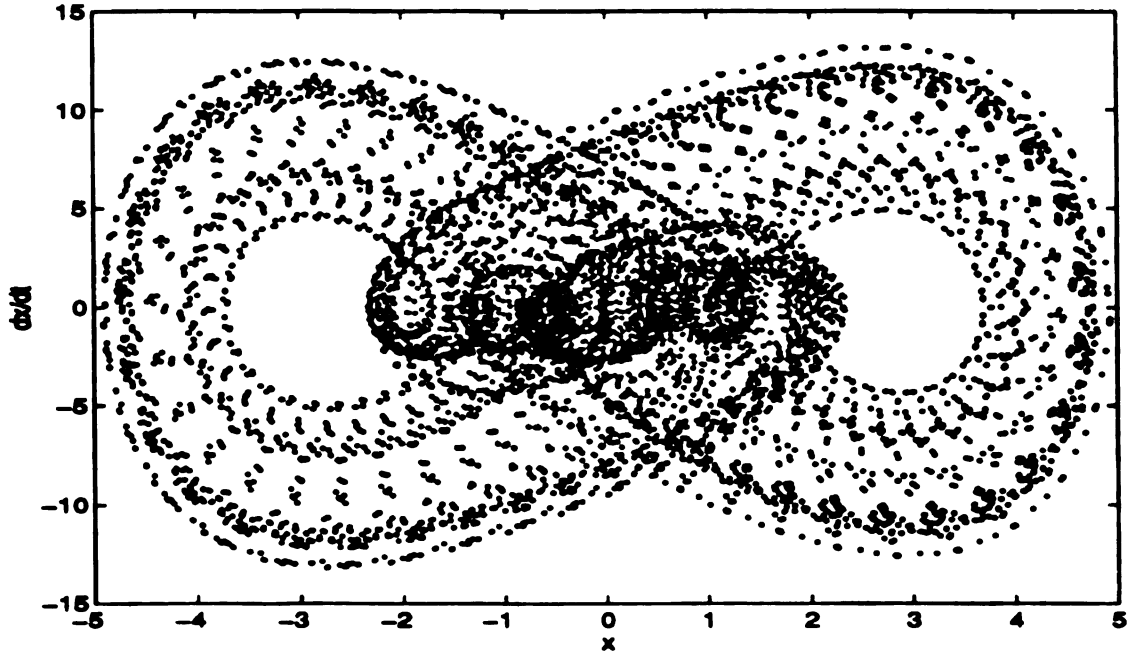


Figure 3.1 Phase portrait of the Duffing oscillator

system of Eq. (3.2) is chaotic, since there is one positive value and the sum of them is negative. (There is a zero exponent from the computer code, corresponding to the time variable of the vector field. We omit it for convenience).

3.1.1 Extraction of the Periodic Orbits

The unstable periodic orbits can be extracted using the recurrence property of the chaotic attractor, as stated in previous chapter. We repeat the idea here to emphasize its importance. We scan the data set in state space forward to locate the recurrent points that are close within a spatial distance ϵ , such that

$$\|x_{i+K} - x_i\| \leq \epsilon \quad (3.3)$$

for a periodic orbit with K data points in the orbit. Here the index i is taken as the phase angle of the periodic orbit relative to the forcing function, which is to be used in the

calculat

span of

dx/dt

dx/dt

3.1.2

To ide

essenti

system

externa

polynor

systems

calculation of the Fourier coefficients. The spatial distance ε is chosen to be 0.5% of the span of the data set [5,35]. Some of the extracted periodic orbits are shown in Figure 3.2.

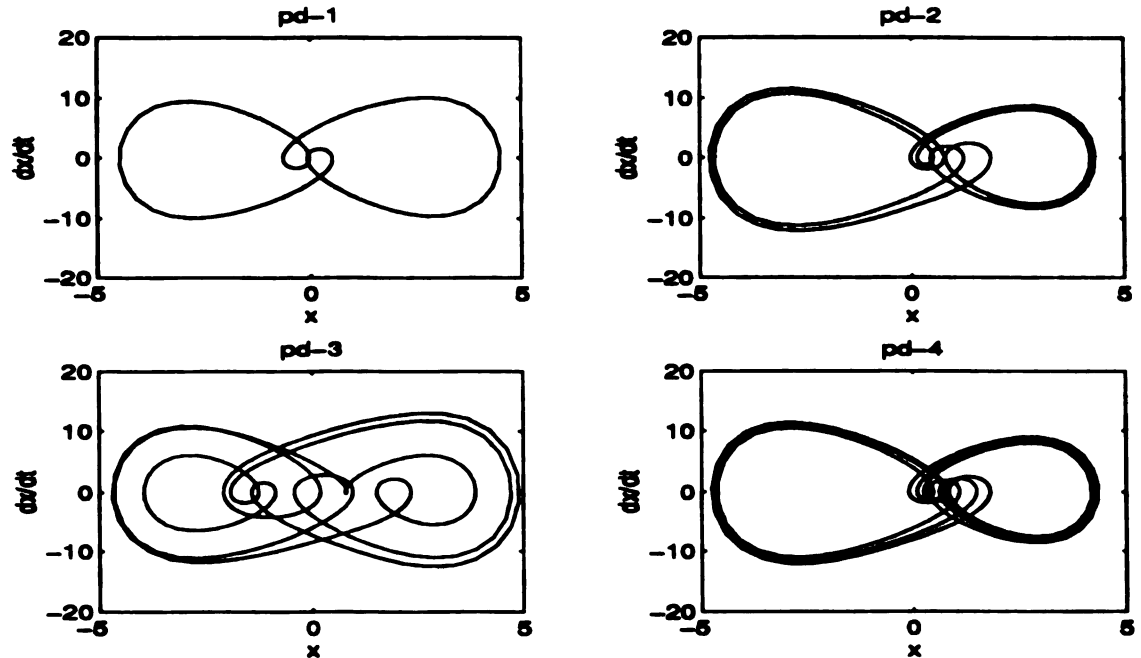


Figure 3.2 Some extracted periodic orbits of the Duffing oscillator

3.1.2 Choosing a Mathematical Model

To identify the system parameters, we need a mathematical model that can catch the essential feature of the original system. Some *a priori* knowledge about the original system will help choosing a valid model. In this case, we know that the system is an externally excited, Duffing-type nonlinear system. Hence we choose a model in polynomial form, which has been commonly used in modeling the Duffing type nonlinear systems. The model with viscous damping is written as

$$m\ddot{x} + \alpha\dot{x} + \sum_{i=1}^p \beta_i x^i = a \cos \omega t, \quad (3.4)$$

where m , α , and β_i are the parameters to be identified.

3.1.3 Identification Results

Applying the extracted periodic-orbit data to the mathematical model of Eq. (3.4), each term in the model is expressed in a Fourier series. The phase angle associated with each periodic orbit is included in the calculation of their Fourier coefficients, as discussed in detail in Chapter Two. Then the principle of harmonic balance is applied to the primary harmonics of the Fourier series, resulting in a set of algebraic equations in system parameters to be estimated by a least-squares fit.

We first apply four sets of the periodic-orbit data separately to the model of Eq. (3.4), with five terms retained in the polynomials, the identification results are shown Table 1.

Also, we apply four sets of periodic-orbit data together to increase the redundancy of the least-squares fit with different number of terms included in the model. The identification results are shown in Table 2.

The results are accurate compared to the actual values, and consistent with each other for using different set of periodic-orbit data. The non-zero parameter values are recovered within 1% of their nominal values, and the zero-valued parameters are close to zero, even when the mathematical model contains many unnecessary high-order nonlinear terms. The standard deviations are less than 1% of the non-zero parameter values, or close to the average values of the zero-valued parameters, indicating the consistency of the results. Combining individual sets of algebraic equations increases the redundancy in the least-

Table

period
orbi

actu.

pd-

pd-

pd-

pd-

Avera

std. d

square.

include

The id

nonline

terms i

3.1.4

From t

the ide

extract

unstab

Table 1: Identification results using individual periodic orbit for Duffing's equation

periodic orbits	m	α	β_1	β_2	β_3	β_4	β_5
actual	1.0000	.2000	1.0000	0.0000	1.0000	0.0000	0.0000
pd-3	0.9999	.1997	0.9915	-.0023	1.0009	.0002	.0000
pd-4	1.0008	.2002	1.0498	-.0050	0.9803	.0007	.0010
pd-5	0.9997	.1998	0.9659	-.0020	1.0124	.0001	-.0006
pd-6	1.0001	.1999	1.0015	.0016	1.0009	-.0002	-.0061
Average	1.0001	.1999	1.0022	-.0019	0.9968	.0002	-.0014
std. dev.	0.0005	.0002	0.0351	.0027	0.0134	.0004	.0032

squares fit, and improves the accuracy of the identification results when the model includes many parameters.

The identified results suggest that the model can be refined by removing the higher-order nonlinear terms whose parameter values are negligible. The reduction of the unnecessary terms in the model tends to yield higher accuracy in the identification results.

3.1.4 Model Verification

From the numerical results, the model of Eq. (3.4) can be easily verified. However, we use the identified model with the average values in Table 2 to generate a set of data, and extract the unstable periodic orbits, for comparison with the original ones. The extracted unstable periodic orbits from the identified model are shown in Figure 3.3. They resemble

Table 2: Identification results using 4 periodic orbits for Duffing's equation

orders	m	α	β_1	β_2	β_3	β_4	β_5	β_6	β_7
actual	1.000	.2000	1.000	0.000	1.000	0.000	0.000	0.000	0.000
p=4	1.000	0.200	1.005	-0.001	1.000	0.000			
p=5	1.000	0.200	1.015	-0.001	0.996	0.000	0.000		
p=6	1.000	0.200	1.010	0.004	0.998	-0.001	0.000	0.000	
p=7	1.000	0.200	1.005	0.004	1.000	-0.001	0.000	0.000	-0.000
Avg.	1.000	0.200	1.009	.0015	0.999	-.001	0.000	0.000	0.000
std.dv	0.000	0.000	0.005	0.003	0.002	0.001	0.000	0.000	0.000

closely their counterparts in Figure 3.1 and Figure 3.2.

The bifurcation diagrams, as shown in Figure 3.4, are calculated using the original equation and the identified one, by slowly increasing the forcing amplitude and sampling the steady-state response at the same Poincare section. The resemblance of the original bifurcation diagram and the identified one can be clearly seen.

The Lyapunov exponents of the identified model calculated by the computer code of Wolf *et al.* [58] are convergent to $\tilde{\lambda}_1 = 0.20$, and $\tilde{\lambda}_2 = -0.49$, which are close to the original values of $\lambda_1 = 0.18$ and $\lambda_2 = -0.468$, with deviations of 11.1% and 4.7% respectively.

Thus our model is verified.

3.1.5 Effect of Noise

Numerically generated data are considered to be essentially noise free. The excellent

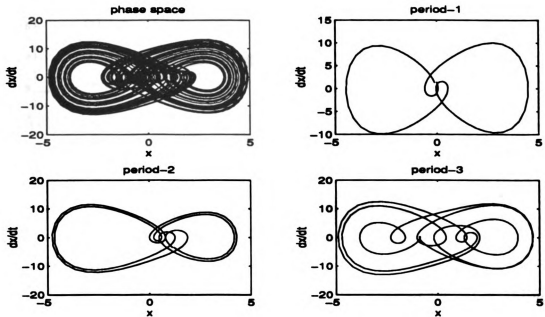


Figure 3.3 The simulated chaotic attractor and some of the extracted periodic orbits of the identified model

identification results in the example above may deteriorate if noise is present in the periodic data. To assess the influence of noise on the identification results, a set of uniformly-distributed random noise is added to each periodic orbit for use in the identification algorithm to test sensitivity of A , q and $A\alpha = q$. If the noise is added to the chaotic set before the extraction of the periodic orbits, the spatial criterion ϵ may need an adjustment.

The noise level is set by the ratio of its maximum amplitude to that of the employed periodic-orbit data. Figure 3.5(a) shows a period-3 noise-free periodic orbit and Figure 3.5(b) shows its 2% noise contaminated counterpart in phase space. We examine the noise

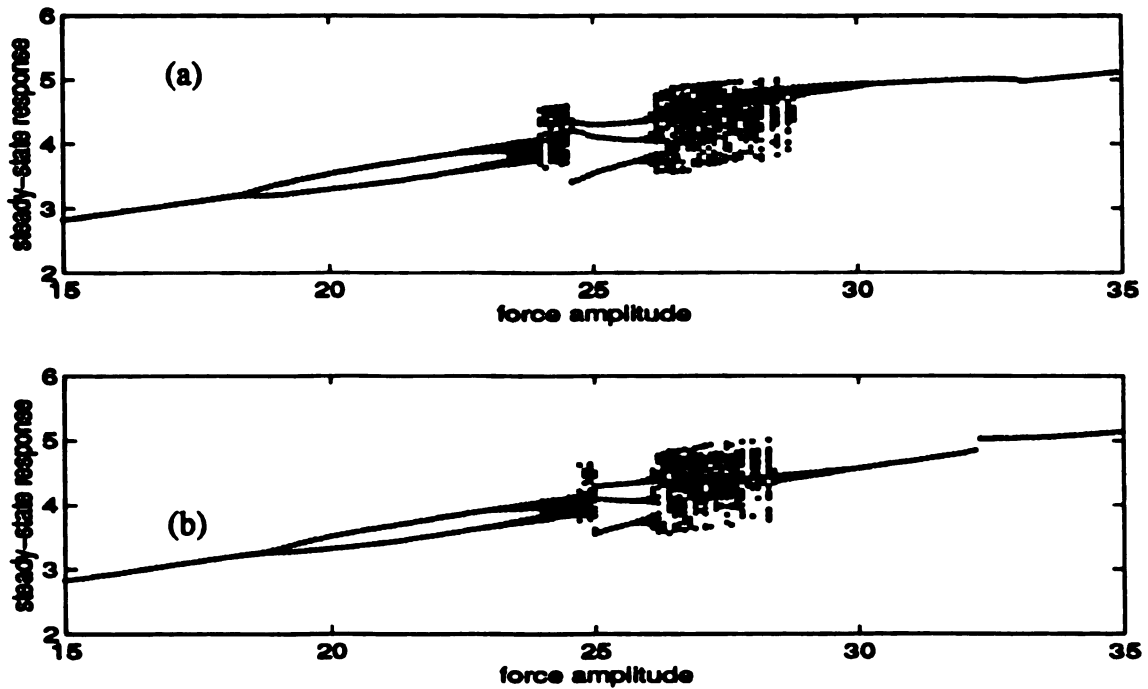


Figure 3.4 Bifurcation diagrams of the Duffing's equation (a) using the original equation, and (b) using the identified model with the average values in Table 2

effect by using the model (3.4) with varying nonlinear terms and varying noise levels. Four sets of noisy periodic-orbit data are used together in the identification algorithm. The identification results are shown in Table 3.

Comparing with the previous results in Table 2 for the same model, we find that,

- (1) within 5% noise level, the noise effect is not significant for a model with three or four terms in the polynomial. As the nonlinear terms increase beyond five, the noise effect increases. The errors are within 2.3% of the non-zero parameters. The zero-valued parameters have larger deviations than in previous case;
- (2) For the nonlinear terms in the model are greater than five, the noise effect increase rapidly, resulting in less accurate identification results. The issue of noise will be

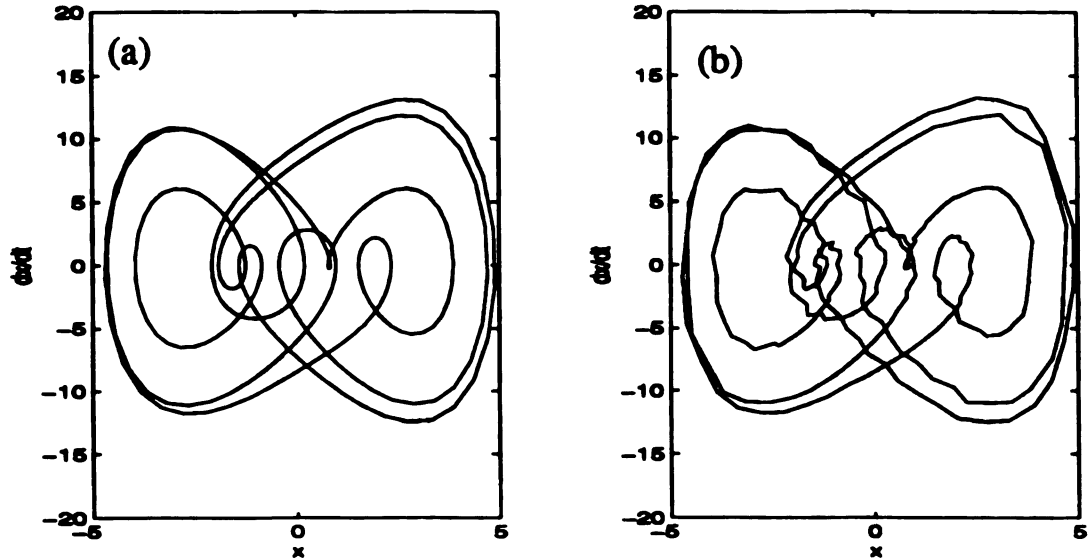


Figure 3.5 (a) A noise-free periodic orbit, (b) the noise-contaminated counterpart

discussed in Chapter Five;

(3) For a small amount of noise, the effect of noise is not catastrophic to our method, but in a robust way.

With the model identified using the noisy periodic data, we proceed to verify the model by comparing the Lyapunov exponents, the structure of the unstable orbits, and the bifurcation diagrams as before. Using a model with the parameter values as in the last second row of Table 3, the Lyapunov exponents calculated by the computer code of Wolf *et al.* [58] are convergent to $\tilde{\lambda}_1 = 0.21$, and $\tilde{\lambda}_2 = -0.5$, which are close to the original values of $\lambda_1 = 0.18$ and $\lambda_2 = -0.468$, with deviations of 16.67% and 6.84% respectively.

The simulated chaotic attractor and the extracted periodic orbits from the identified model

Table 3: Identification results for Duffing's equation using noisy data

noise	orders	m	α	β_1	β_2	β_3	β_4	β_5
	actual	1.000	.200	1.000	0.000	1.000	0.000	0.000
1%	p=3	1.000	.200	0.999	-.006	1.000		
1%	p=4	1.000	.200	1.000	-.001	1.000	.000	
1%	p=5	1.000	.200	1.058	.016	0.983	.001	.001
2%	p=3	1.000	.200	0.999	-.013	1.002		
2%	p=4	1.000	.200	1.004	-.029	1.001	.001	
2%	p=5	1.001	.201	0.947	.016	1.036	-.009	-.005
3%	p=3	1.000	.200	0.995	-.020	1.002		
3%	p=4	1.000	.200	1.002	-.042	1.001	.001	
3%	p=5	1.001	.201	1.136	-.044	0.958	.002	.002
5%	p=3	1.000	.200	0.977	-.032	1.002		
5%	p=4	0.999	.200	0.988	-.069	1.001	.002	
5%	p=5	1.001	.201	1.202	-.073	0.931	.003	.003

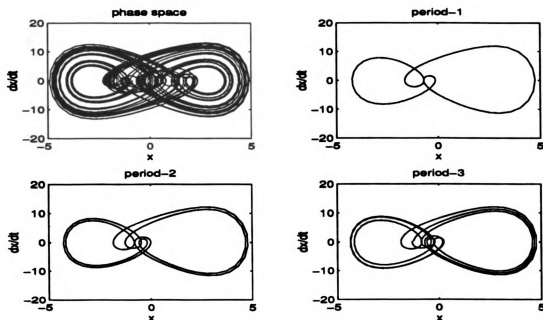


Figure 3.6 The simulated chaotic attractor and some of the extracted periodic orbits of the identified model using the noise-contaminated periodic orbits

are shown in Figure 3.6. The qualitative resemblance with the original ones of Figure 3.1 and Figure 3.2 is clearly seen.

A bifurcation diagram is constructed for the identified model, by slowly increasing the force amplitude as the control parameter, and sampling the steady-state response at the same time interval, as shown in Figure 3.7(b). It closely resembles the original one in Figure 3.7(a). Thus the model is verified.

3.2 A Smooth Coulomb Friction System

A smooth Coulomb friction system is given as

$$\ddot{x} + c\dot{x} + x + (1 + kx) \tanh(ax) = f \cos(\omega t), \quad (3.5)$$

which is one of the models of a dry-friction system, studied extensively by Feeny and

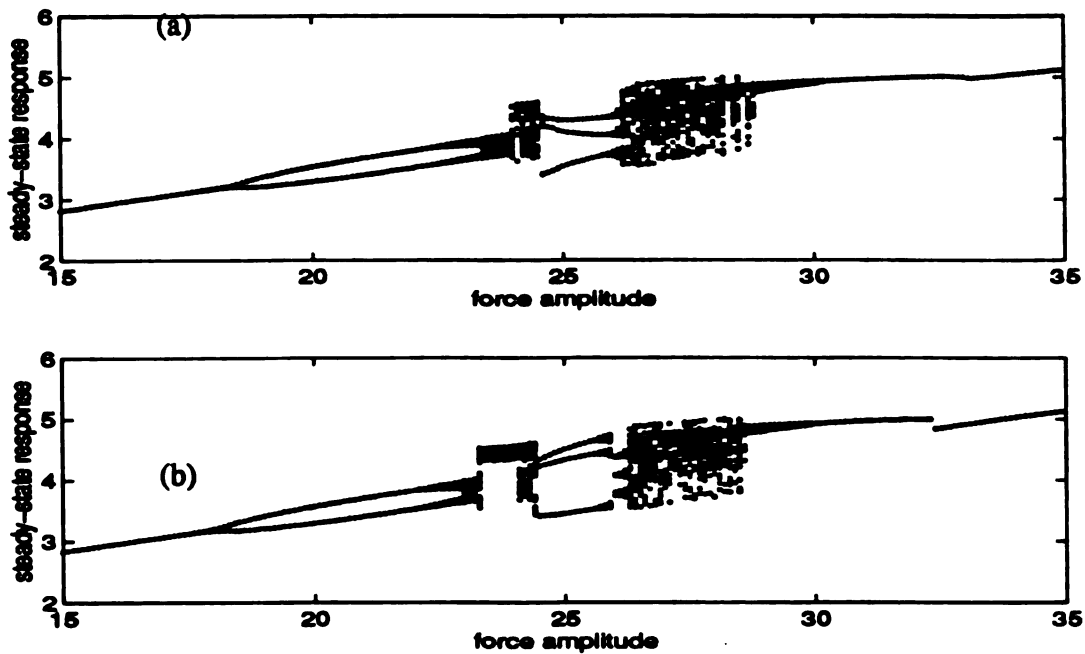


Figure 3.7 Bifurcation diagrams of the Duffing's equation (a) using the original equation, (b) using the identified model of the noisy case

Moon [24]. The dry-friction is often modeled as a multivalued, discontinuous nonlinear force, which causes a “stick-slip” chaotic motion in a large parameter space. Here, the smooth function, $\tanh(ax)$, is used to approximate the Coulomb friction model. This system exhibits ‘almost sticking’ motions, featuring a funnel-like structure in the phase space under the harmonic excitation [24]. We choose the parameter values as $c = 0.03$, $k = 1.5$, $a = 50$, and the forcing term as $1.9 \cos(1.3t)$, for numerical simulation. Numerical integration is carried out by a 5th-order Runge-Kutta method as before. A two-dimensional phase portrait is shown in Figure 3.8, where a funnel-like structure is clearly seen.

The Lyapunov exponents are calculated from the known equation using the computer code

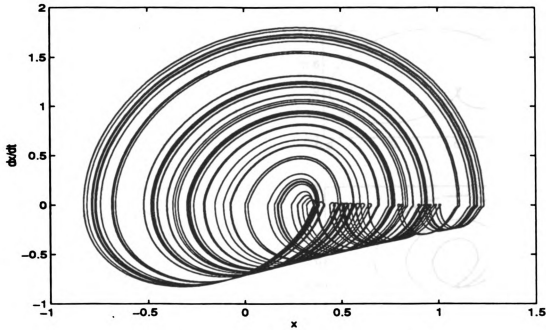


Figure 3.8 Phase portrait of a Coulomb friction system

by Wolf *et al.* [58], which converge to $\lambda_1 = 0.13$ and $\lambda_2 = -39.8$, indicating that the system is chaotic indeed.

To proceed identifying the parameters of this chaotic system, we look for the periodic orbits embedded within the chaotic set. Using the procedures stated previously, some of the unstable periodic orbits are extracted, as shown in Figure 3.9.

Also we choose a model in a polynomial form as that of Eq. (3.4), assuming no knowledge about the nonlinear function of the system. But, after conducting the identification procedures, we found that the identification results were very poor. We postulate that the power series representation of the nonlinear function, $\tanh(ax)$, may not be valid with the numerical data, due to the large value of $a = 50$. We then choose another model that

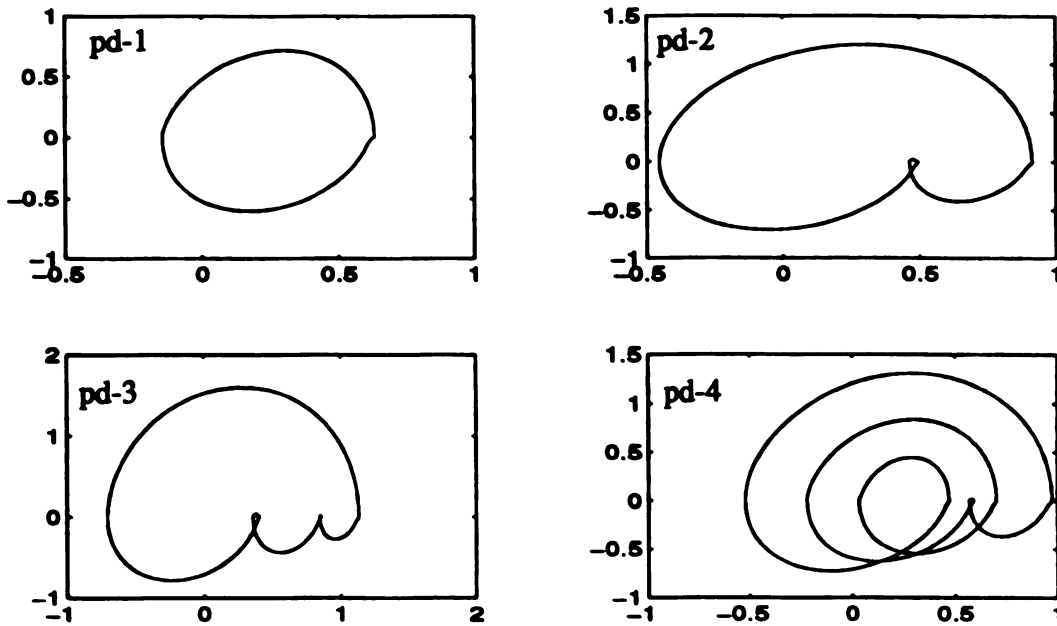


Figure 3.9 Some extracted periodic orbits of a Coulomb friction system

contains the smooth function as a known function, such as

$$m\ddot{x} + c\dot{x} + \sum_{i=1}^P \alpha_i x^i + \sum_{i=1}^P \left(\beta_i x^{i-1} \right) \tanh(ax) = f \cos(\omega t). \quad (3.6)$$

Applying four sets of the periodic orbits to this model with different numbers of nonlinear terms retained, the identification results are shown in Table 4.

Up to the nonlinear order of five in the mathematical model, the parameters identified are accurate within 1.0% error, with the standard deviation less than 1.0% of the non-zero parameters or close to the average identified values of the zero-valued parameters.

The identified results suggest that the model can be refined by the same procedure as in previous case. By removing the high-order nonlinear terms whose parameter values are

Table 4: Identification results using 4 periodic orbits for Coulomb friction system

p	m	c	α_1	α_2	α_3	α_4	β_1	β_2	β_3	β_4
real	1.000	.0300	1.000	.0000	.0000	.0000	1.000	1.500	.0000	.0000
p=3	.9977	.0291	.9997	.0086	-.016		1.002	1.501	-.009	
p=4	.9971	.0294	.9904	.0192	.0036	-.021	1.002	1.503	-.006	-.008
p=5 ^a	.993	.030	.970	.030	.0170	-.021	1.000	1.515	-.000	-.036
avg.	.996	.0295	.9867	.0193	.0015	-.021	1.001	1.506	-.005	-.022
std.	.002	.0004	.0152	.0107	.0166	.000	.0011	.0076	.0046	.0198

a. $\alpha_3 = -0.003$ and $\beta_3 = 0.009$

negligible, the accuracy of identification results is improved, and the consistency remains. The model can be verified by the same criteria used in the previous case also. From the numerical results that the identified values are close to the real ones within 1%, we expect to get similar results, and reluctantly omit them here.

3.2.1 Effect of Noise

We wonder how noise will affect the identification results of this system. We add the uniformly-distributed random noise to the periodic orbit for use in the identification algorithm. Three sets of periodic-orbit data are applied to the chosen model of Eq. (3.6).

Parameter identification results are shown in Table 5.

We find that the noise deteriorates the accuracy of the parameter identification results rapidly when the noise level is increased. Due to the large parameter value in the hyper-

Table 5: Noise effect on identification results for Coulomb friction system

noise level	orders	m	c	α_1	α_2	α_3	β_1	β_2	β_3
	real	1.000	0.030	1.000	0.000	.000	1.000	1.500	0.00
1%	p=2	1.002	0.093	0.998	-.021		0.968	1.508	
1%	p=2	0.994	0.165	0.96	-.005		0.933	1.515	
2%	p=3	0.996	0.084	1.019	0.017	-.083	0.979	1.518	-.041
2%	p=3	0.982	0.150	1.004	0.072	-.168	0.953	1.532	-.074

tangent function, $\tanh(ax)$, the noise amplitude has been amplified significantly, such that the accuracy of the identification results may have been distorted. This is a case in which sensor noise may cause trouble in obtaining accurate identification results.

3.3 A Parametrically Excited System

The numerical example for a parametrically excited system is a nonlinear Mathieu equation, given as [13]

$$m\ddot{x} + c\dot{x} + (\beta + a \sin \omega t)x + \nu(\gamma - a \sin \omega t)x^3 = 0. \quad (3.7)$$

This is a model of an inverted pendulum under a two-well potential generated from above by a magnetic dipole, studied experimentally by Cusumano and Sharkady [13] for the bifurcation and low-order modeling of a parametrically excited system. The pendulum can be buckled and unbuckled by changing the voltage applied to the electromagnet. It is also an example of a periodically disappearing separatrix, analyzed previously by Coppola and

Rand [10], and Bridge and Rand [8].

The parameter values used to generate the chaotic data are $m = 1$, $c = 0.01$, $\beta = 0.25$, $\gamma = 0.75$, $\nu = 1/3$, and the parametric forcing function is $0.55 \sin(0.28t)$ [13]. Numerical integration of the governing equations is carried out by a 5th-order Runge-Kutta method on a Sun workstation as before. The phase portrait is constructed using the numerical data, as shown in Figure 3.10, from which the unstable periodic orbits are extracted, as shown in Figure 3.11.

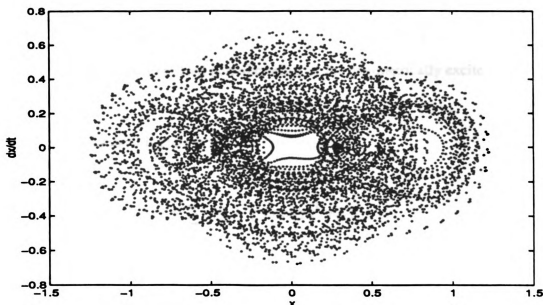


Figure 3.10 Phase portrait of the parametrically excited system

The Lyapunov exponents are calculated using the computer code by Wolf *et al.* [58], and converge to $\lambda_1 = 2.03$ and $\lambda_2 = -32.35$, indicating that the nonlinear system of Eq.(3.7) is chaotic indeed.

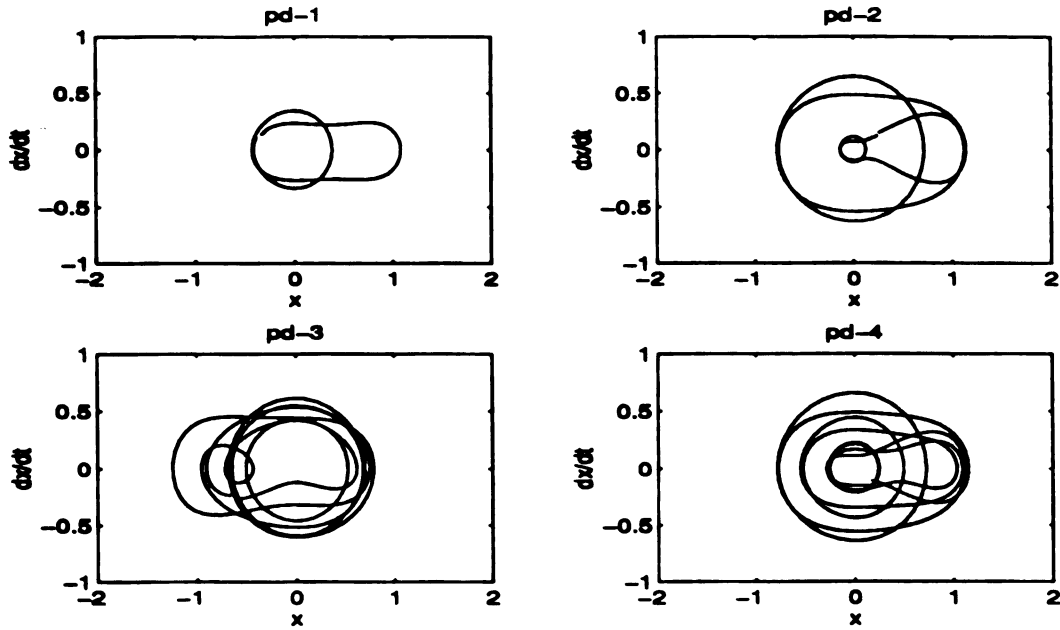


Figure 3.11 Some extracted periodic orbits of the parametrically excited system

The mathematical model is chosen as

$$c\dot{x} + \sum_{i=1}^p (\beta_i + \gamma_i \sin \omega t) x^i = -x. \quad (3.8)$$

Here, the x -term is taken as a known quantity based on fact that the periodic solution is known by the extracted periodic orbit data. Using these periodic orbits, each term in the model is expressed in a Fourier series, with the parametrically excited force being combined with the x -term as a single function. Applying the principle of harmonic balance to each harmonic of the Fourier series, a set of algebraic equations in system parameters is formed. Four sets of periodic-orbit data are used to increase the redundancy of the algebraic equations, and the identification results are shown in Table 6, for different numbers of nonlinear terms retained in the model.

Table 6: Identification results using 4 periodic orbits for a parametrically excited system

	c	β_1	β_2	β_3	β_4	β_5	γ_1	γ_2	γ_3	γ_4	γ_5
real	0.01	0.25	0.00	0.25	0.00	0.00	0.55	0.00	-	0.00	0.00
p=3	.011	.250	.001	.254			.550	-.00	-		
p=4	.011	.250	-.00	.252	.011		.550	-.00	-	.010	
p=5	.011	.249	-.01	.249	.018	.012	.559	-.00	-	.022	.034
Avg.	.011	.250	.004	.252	.015	.012	.553	-.00	-	-	.034
std.	.000	.001	.006	.003	.004	.00	.004	.00	.021	.033	.000

The results are accurate compared to the real values for the number of nonlinear terms in the model is not excessively large, such as the first two cases in the table (p=3 and p=4). The non-zero parameters are close to the actual values, with less than 1% error of the nominal parameter values, and the zero-value parameters are close to zero.

As the number of the nonlinear terms in the model increases, the identified parameters that are coupled with forcing function are less accurate. Among the parameters, the damping is small in value and vulnerable to numerical errors. In this case, perhaps the damping should be estimated independently by traditional method, or using the global estimation method proposed by Cusumano and Kimble [12].

Refining the model by removing the high-order nonlinear terms with negligible values, the

accuracy is improved. We expect the model verification will be satisfactory for this parametrically excited system, as demonstrated by the example in section 3.1.

3.3.1 Effect of Noise

To assess the influence of noise on the identification results, the set of uniformly-distributed random noise generated before is added to the periodic orbits for use in the identification algorithm. The noise level is set as the percentage of the maximum amplitude of the employed periodic data. Applying four sets of the contaminated periodic-orbit data to the model of Eq. (3.8) with varying nonlinear orders, the identification results are shown in Table 7.

Compared with the noise-free cases in Table 6, the effect of noise on the identification results are not significant for three or four nonlinear terms retained in the mathematical model. It becomes more significant when high-order nonlinear terms are included in the model and higher level of noise is added to the periodic orbits. Up to the noise level of 3% of the employed periodic data, identification results are acceptable.

3.4 An Autonomous System: the Lorenz Equations

We take the Lorenz equation as an example of an autonomous chaotic system, written as

$$\begin{aligned}\dot{x}_1 &= \sigma(x_2 - x_1) \\ \dot{x}_2 &= \rho x_1 - x_2 - x_1 x_3 \\ \dot{x}_3 &= -\beta x_3 + x_1 x_2\end{aligned}\tag{3.9}$$

with the parameter values as $\sigma = 16$, $\rho = 45.92$, and $\beta = -4$. Numerical data are generated from Eq. (3.9) using a 5th-order Runge-Kutta method for 10000 data points with time interval being 0.025sec. There exists a 'butterfly shaped' chaotic attractor, as

Table 7: Noise effect on identification results for a parametrically excited system

		c	β_1	β_2	β_3	β_4	β_5	γ_1	γ_2	γ_3^a	γ_4	γ_5
	real	.010	.250	.000	.250	.000	.000	.550	.000	.183	.000	.000
1%	p=3	.011	.250	-.00	.253			.547	.001	.177		
1%	p=4	.011	.251	-.01	.252	.01		.547	-.00	.177	.01	
1%	p=5	.011	.251	-.01	.243	.01	.02	.553	-.00	.208	.01	.03
2%	p=3	.011	.251	-.00	.253			.544	-.00	.173		
2%	p=4	.011	.251	-.01	.252	.01		.544	-.00	.173	.01	
2%	p=5	.011	.253	-.01	.238	.01	.02	.548	-.00	.195	.01	.02
3%	p=3	.011	.251	-.00	.253			.541	-.00	.168		
3%	p=4	.011	.252	-.01	.252	.01		.541	-.00	.168	.01	
3%	p=5	.011	.254	-.01	.234	.00	.02	.543	-.00	.183	.00	.02
5%	p=3	.011	.251	-.01	.254			.535	-.00	.158		
5%	p=4	.011	.252	-.01	.252	.01		.535	-.00	.158	.01	
5%	p=5	.011	.257	-.01	.227	-.00	.02	.533	-.00	.159	-.01	.01

a. negative values as in the problem setting.

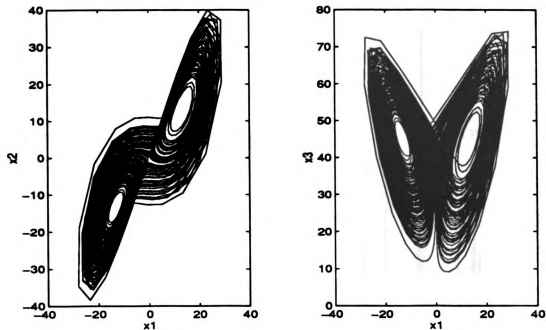


Figure 3.12 Phase portrait of a Lorenz system

shown in Figure 3.12, in which infinitely many unstable periodic orbits are dense and have an incommensurate period associated with each periodic orbit.

Since the system is unforced, there is no fundamental period to be used as a guide for finding the unstable periodic orbits for use in our parametric identification scheme. We use the recurrence property of the chaotic attractor to construct a recurrence plot to determine the period length of the periodic orbits, as stated in detail in Chapter Two. The recurrence plot is shown in Figure 3.13, in which the recurrent points that are clustered around certain values can be clearly seen. These values indicate the incommensurate periods of the periodic orbits. Using the values, the corresponding periodic orbits can be located within the Lorenz attractor. Some of the extracted periodic orbits are shown in Figure 3.14, which

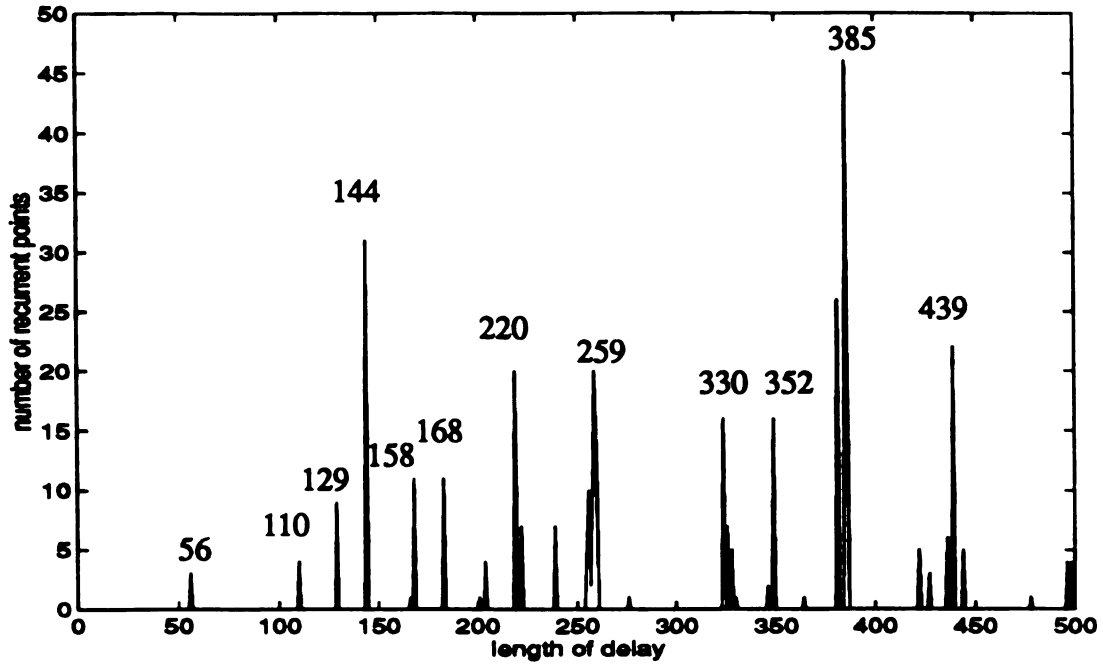


Figure 3.13 Recurrence plot of the Lorenz system (period lengths are indicated in the numbers of time steps used in the numerical integration)

are to be used in our identification algorithm.

Knowing that the system is a Lorenz type autonomous system, a mathematical model is chosen such that the linear terms and the quadratic nonlinear terms are included as

$$\dot{x}_1 = \sum_{i=1}^3 \left(a_{1i} x_i + \sum_{j \geq i}^3 b_{ij} x_i x_j \right) \quad (3.10)$$

$$\dot{x}_2 = \sum_{i=1}^3 \left(a_{2i} x_i + \sum_{j \geq i}^3 c_{ij} x_i x_j \right) \quad (3.11)$$

$$\dot{x}_3 = \sum_{i=1}^3 \left(a_{3i} x_i + \sum_{j \geq i}^3 d_{ij} x_i x_j \right). \quad (3.12)$$

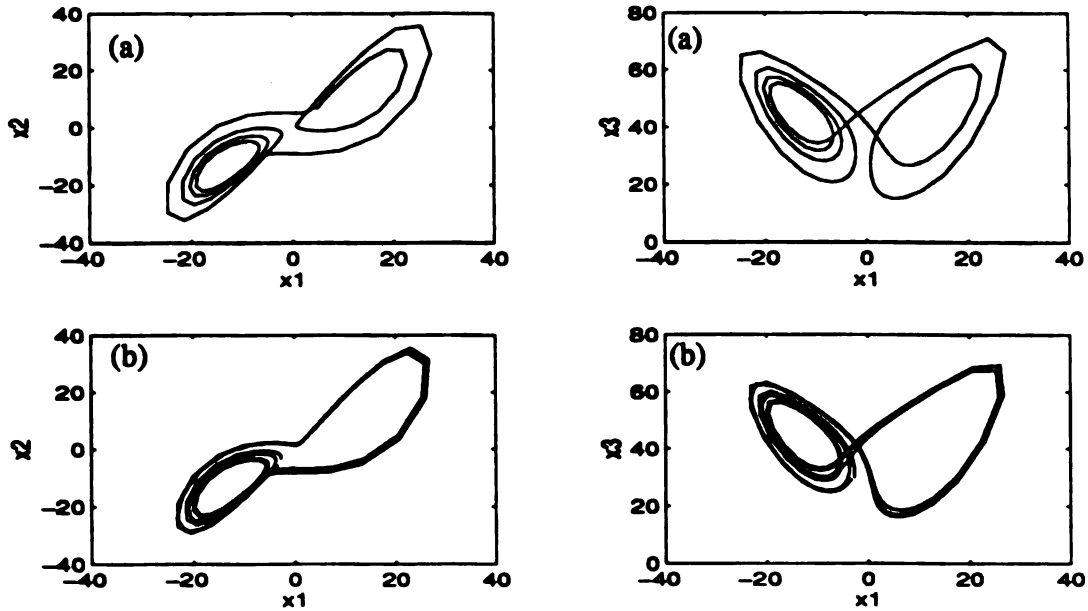


Figure 3.14 Two extracted periodic orbits of a Lorenz system: (a) period length of 110 time steps, (b) period length of 144 time steps

where a_{ij} , b_{ij} , c_{ij} , and d_{ij} are the parameters to be determined.

Using the periodic orbits, each term in the model is expressed in a Fourier series with the fundamental period obtained from the recurrence plot. The Fourier coefficients are calculated as before, except the phase angle is ignored, due to the fact that there is no forcing function involved. By balancing the Fourier coefficients of each harmonic in each equation, and treating the \dot{x}_i -terms as known quantities, a set of algebraic equations in system parameters is constructed for the least-squares estimation.

We use two periodic orbits with period lengths of 110 time steps and 144 time steps respectively, as shown in Figure 3.14, in the identification algorithm. The estimated parameter values are shown in Table 8.

Table 8: Identification results for the Lorenz equation^a (a)

	x_1	x_2	x_3	x_1x_1	x_1x_2	x_1x_3	x_2x_2	x_2x_3	x_3x_3
\dot{x}_1	-15.951 (-16.0)	15.971 (16.0)	-0.098	-0.030	.019	-.003	.000	.003	.003
\dot{x}_2	45.748 (45.92)	-.927 (-1.0)	.230	.039	-.028	-.995 (-1.0)	.003	-.004	-.006
\dot{x}_3	-.089	.041	-3.877 (-4.0)	.031	.980 (1.0)	.003	.000	-0.003	-.004

a. The values are the parameter values of each equation in Eq. (3.12) indicated by the first column.

The actual parameters presented in the original system are identified accurately as highlighted in bold-face in the table, although some of the zero-valued parameters are not close to zero, such as the third term in the second equation.

The model equation of (3.12) can be refined by knowing that there is no ‘square’ term in the Lorenz equation. This refinement improves the accuracy of the identification results significantly, not only the non-zero parameters are closer to the real values, but also the zero-valued parameters are close to zero, as shown in Table 9.

3.4.1 Effect of Noise

To assess the influence of noise on the identification results, we add a set of uniformly-distributed random noise to the periodic orbits as before. With 1% noise added to the extracted periodic orbits, the identification results of the model without square-terms are not significantly affected, although some of the zero-value terms have non-zero values, as shown in Table 10. With higher-level noise added to the periodic orbits, the identification

results deteriorate rapidly. This case shows that noise is influential to the parametric identification results for the autonomous system.

Table 9: identification results for Lorenz equation^a (b)

	x_1	x_2	x_3	x_1x_2	x_1x_3	x_2x_3
\dot{x}_1	-16.011 (-16.0)	15.953 (16.0)	-0.006	0.001	0.0002	0.0011
\dot{x}_2	45.900 (45.92)	-1.0228 (-1.0)	-0.0127	0.0020	-0.9996 (-1.0)	0.0021
\dot{x}_3	0.0041	0.007	-3.9991 (-4.0)	0.9999 (1.0)	-0.0001	-0.0002

a. The values are the parameter values of each equation in Eq. (3.12) as indicated by the first column without the square terms in the model.

Table 10: Identification results for Lorenz equation^a with 1% noise

	x_1	x_2	x_3	x_1x_2	x_1x_3	x_2x_3
\dot{x}_1	-15.5813 (-16.0)	15.9582 (16.0)	0.0757	0.0006	-0.0087	0.0011
\dot{x}_2	47.4206 (45.92)	-1.8632 (-1.0)	0.0256	0.0034	-1.0252 (-1.0)	0.0112
\dot{x}_3	-0.9178	0.5717	-3.9468 (-4.0)	0.9902 (1.0)	0.0200	-0.0129

a. The values are the parameter values of each equation in Eq. (3.12) as indicated by the first column without the square terms in the model.

3.5 A Case Study on Modeling the Nonlinearity with a Power Series

We have confronted a problem in modeling a hyperbolic-tangent function with a power

series in Coulomb-friction system. We postulate that the power series representation may not be valid in such case. We examine this problem by a similar example, written as

$$\ddot{x} + c\dot{x} + x + k \tanh(x) = f \cos(\omega t) \quad (3.13)$$

We want to show that, if the nonlinear function is known, our method is capable of identifying the parameters accurately, as shown in section 3.2; if the nonlinear function is unknown, and the power series is used to approximate it, then the radius of convergence of the power series and the truncated series representation are the factors influential to the identification results.

The parameter values in Eq. (3.13) are chosen as $c = 0.3$, $k = 0.5$, and $\omega = 1.3$. Numerical data are generated using the Runge-Kutta method with several forcing amplitudes. The maximum periodic responses under different forcing amplitudes are listed in Table 11.

Table 11: Force and response in model (3.13)

case	force, f	max. x
a	0.1	0.25
b	0.5	1.0
c	1.0	2.0
d	2.0	3.0

Note that, by Taylor series expansion, $\tanh(x)$ can be represented by

$$\tanh(x) = x - \frac{1}{3}x^3 + \frac{2}{15}x^5 - \frac{17}{315}x^7 + \dots, |x| \leq \frac{\pi}{2}. \quad (3.14)$$

3.5.1 Using the Known Function in the Model

We choose a mathematical model in a polynomial form as that of Eq. (3.4), with the addition of the known function of $\tanh(x)$ in the model, such that

$$m\ddot{x} + \alpha\dot{x} + \sum_{i=1}^p \beta_i x^i + \gamma \tanh(x) = f \cos(\omega t), \quad (3.15)$$

where the parameters m , α , β_i and γ are to be determined using the periodic data. The identification results are very accurate, as shown in Table 12, even when the mathematical model includes many unnecessary terms.

Table 12: Identification results using the exact function in Model (3.15)

cases	m	α	β_1	β_2	β_3	β_4	β_5	γ
actual	1.0000	0.3000	1.0000	0.0000	0.0000	0.0000	0.0000	0.5000
a~b	1.0006	0.3000	1.0300	-0.0009	-0.0000	0.0000	0.0021	0.4700
a~c	0.9999	0.3000	1.0008	-0.0000	-0.0002	0.0000	0.0000	0.5000
a~d	1.0000	0.3000	1.0000	.0000	.0000	0.0000	0.0000	0.5001

3.5.2 Using the Power Series Approximation

Assuming that the nonlinear function of the system is unknown, our first choice is using a power series to approximate it. Part of the reason is that it is “easier” to fit the nonlinear function with a polynomial, and “possible” when data is within the radius of convergence.

A model is chosen in a polynomial form as

$$m\ddot{x} + \alpha\dot{x} + \sum_{i=1}^P \beta_i x^i = f \cos(\omega t). \quad (3.16)$$

Applying the periodic data to this model, the identification results are liable to errors, depending on the amplitude of the response and the nonlinear terms retained in the model, as shown in Table 13.

Table 13: Identification results using power series^a in Model (3.16)

cases	m	α	β_1	β_2	β_3	β_4	β_5	β_6	β_7	β_8	β_9
a~b	1.01	.300	1.52	.000	-.155	-.000	.036				
a~d	.951	.300	1.35	.000	-.062	-.000	.003				
a~b	.999	.300	1.50	-.000	-.166	.000	.060	-.000	-.014		
a~d	.991	.300	1.46	-.000	-.103	.000	.013	-.000	-.001		
a~b	1.00	.300	1.50	.000	-.167	-.000	.067	.000	-.025	-.000	.005
a~d	1.11	.300	1.51	.000	-.139	-.000	.031	.000	-.003	-.000	.000
actual	1.00	.300	1.50	.000	-.167	.000	.067	.000	-.027	.000	

a. The terms retained in the series is indicated by the last column number.

In each case, better identification results are obtained using the smaller response data (cases a and b), which are within the radius of convergence of the series. The best result is obtained in the last case, in which the smaller response data are used in the model with nine terms included, which almost fits the power series in Eq. (3.14).

Although the nonlinear function of the system is unknown, we may obtain a qualitative feature of the nonlinear function from the identification results. The nonlinear function is plotted using the identified values, as shown in Figure 3.15, in which the qualitative

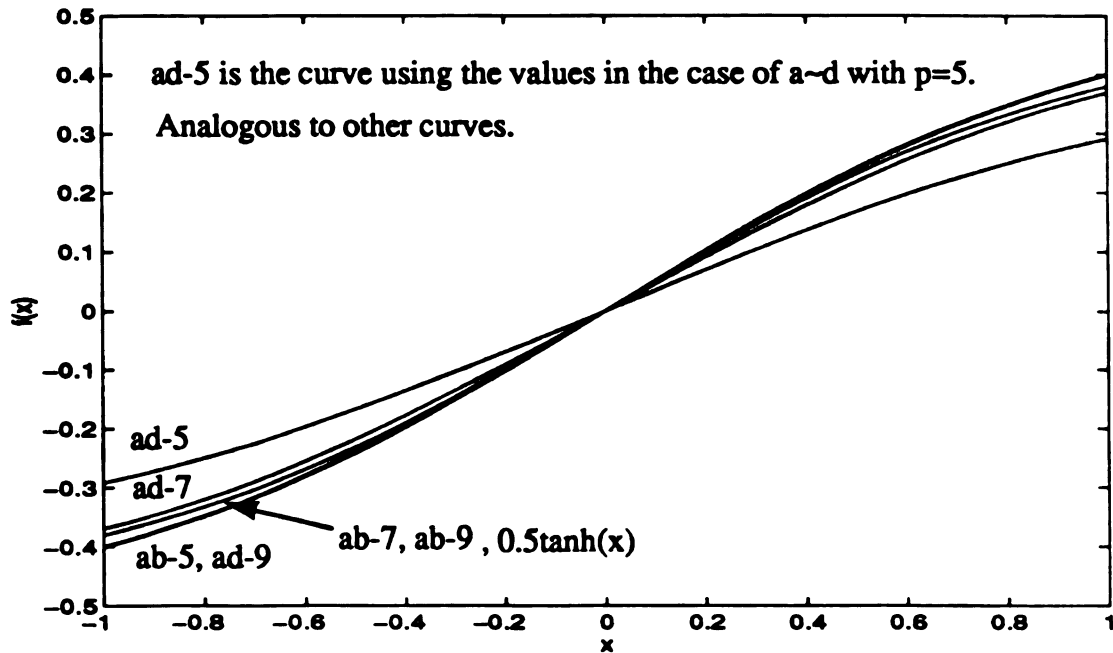


Figure 3.15 Nonlinear function in a power series

feature of the nonlinear function is clearly seen.

3.6 Conclusion

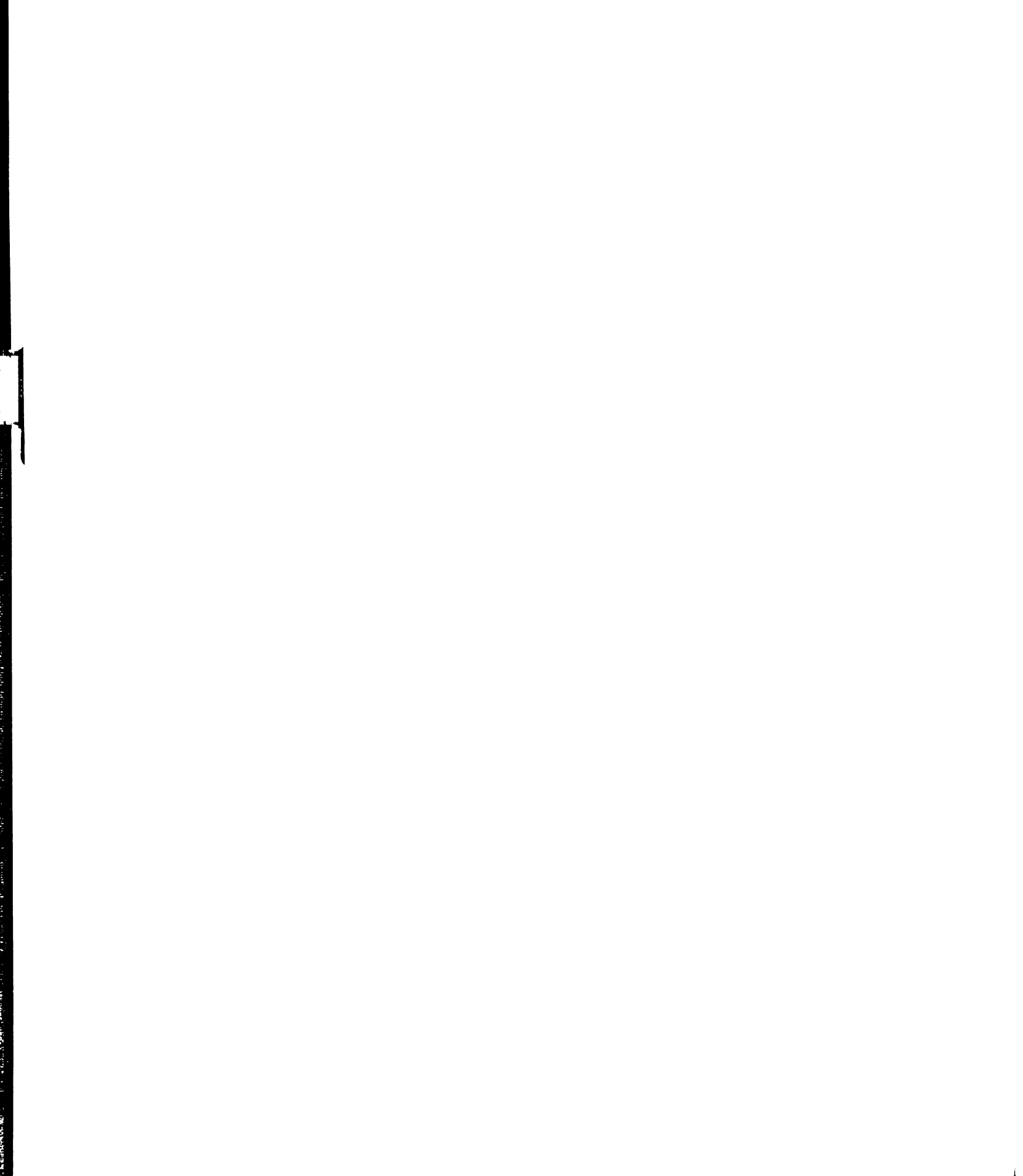
Numerical examples taken from the Duffing's equation, a Coulomb friction system, the nonlinear Mathieu equation, and the Lorenz equation, show that the present method can accurately identify the parameters in a mathematical model that has been well-chosen to match the characteristic of the original chaotic system.

The mathematical model can be refined by removing the unnecessary terms that have negligible values. Consistent identification results are remained for the valid models, implying that the suspicious terms are indeed unnecessary. Models are verified by comparing the structure of the unstable periodic orbits, the Lyapunov exponents, and the bifurcation diagram. The usage of many periodic orbits in the identification scheme

improves the accuracy of the least-squares estimation and provides the statistical information of the identified results. This is suitable for systems with many parameters to be identified.

Random noise added to the periodic orbits can deteriorate the accuracy of the identification results, but in a robust way. This effect worsens when the mathematical models are not well-chosen, for example with many unnecessary terms.

When the precise form of the nonlinearity is unknown, yet smooth, the accuracy of identified truncated power series coefficients deteriorates. However, the truncated power series may be applicable for qualitative modeling.



CHAPTER 4

Experimental Results

4.1 Introduction

In this chapter, we investigate a chaotic data set taken from a periodically driven magneto-oscillator by J. P. Cusumano and B. W. Kimble at Pennsylvania State University. The experiment was designed for observing the global phase-space structure of basins of attraction and homoclinic bifurcation using the stochastic interrogation method [12]. The experimental system was known to be similar to a two-well potential system.

The techniques developed in the previous chapters are to be applied to the given set of chaotic data, in effort to identify the parameters of this experimental system. The chaotic attractor is reconstructed using the method of delays [26, 53], from which the unstable periodic orbits are extracted for use in the identification algorithm. A mathematical model is chosen in polynomial form by knowing that the experimental system has a smooth two-well stiffness potential. The method of harmonic balance is used to form a set of algebraic equations in system parameters, which are estimated by a least-squares fit.

4.2 Experimental Setup

The experiment conducted by Cusumano and Kimble consisted of a stiffened beam

buckled by two magnets. The beam had extra rigidity in the form of steel bars epoxied and bolted along the length away from the clamped end. This additional rigidity was included in effort to make the system behave as a single degree of freedom. The uncovered portion of the beam near the clamped end acted as an elastic hinge from which the position of the beam was measured by a strain gauge. Two rare-earth permanent magnets were placed on the base of the frame holding the beam to create the two-well potential. The frame was then fixed through a rigid mount to an electromagnetic shaker. A periodic driving signal was fed through a power amplifier to the shaker to provide the external forcing function. The experimental set-up is shown in Figure 4.1. [12]

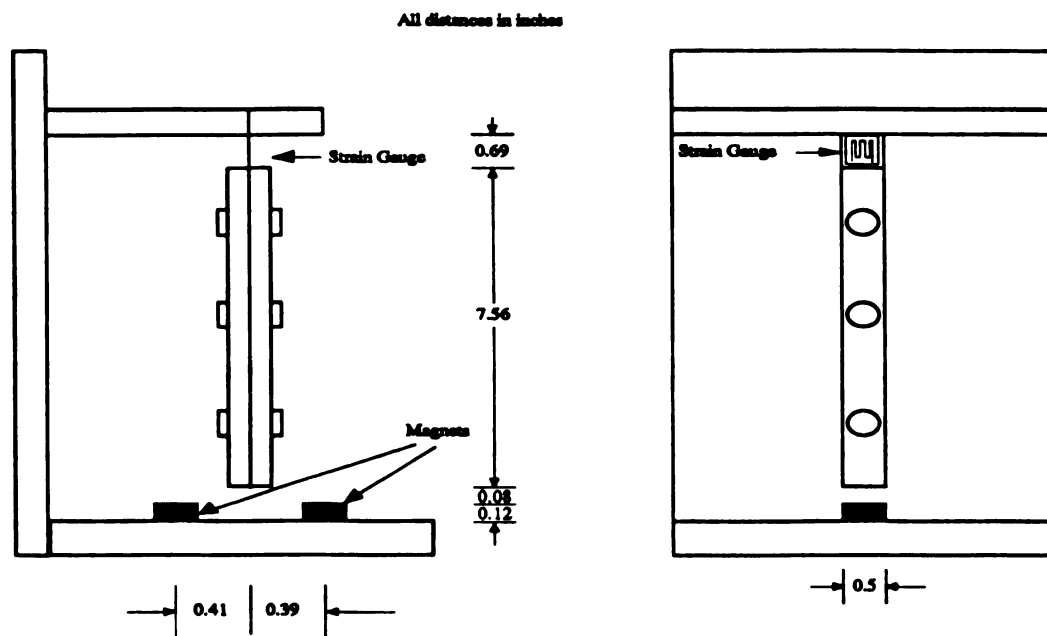


Figure 4.1 Sketch of the experimental setup.

Data from the strain gauge was acquired using a 12-bit data-acquisition (A/D) board, with the digital values from -2408 to 2407 corresponding to -5V to 5V. With no forcing, three equilibria exist; two are stable at digital values of -495 and 315, and one (saddle) is

unstable at approximately zero. When forcing is added, periodic orbits exist instead of equilibrium points. The driving frequency was set at 7.5 Hz with 1.5V of the function generator output, by which the chaotic data were generated and collected at the sampling frequency of 187.5 Hz for 7000 periods of excitation.

4.3 Phase-Space Reconstruction

Since there is only one observable in the data set, denoted by $\{x_j\}, j = 1, \dots, N$, with $x_j = x(j\Delta t)$, Δt is the sampling time interval, the phase space of the experimental system is to be reconstructed. The most common method of phase space reconstruction is the method of delays [26, 53]. It is used to construct a d -dimensional pseudo-vector with its elements being the single observable separated by a constant delay time, such that

$$y_j = \left(x_j, x_{j+\tau}, \dots, x_{j+\tau(d-1)} \right), \quad (4.1)$$

where τ is the delay time, and d is embedding dimension. Both of which are to be determined. The pseudo-vector represents a data point in the embedding space.

In theory, for any sufficiently large dimension d and almost any choice of delay time τ , an *embedding* of the original attractor can be obtained, and the geometrical invariants such as dimension and positive Lyapunov exponents can be preserved. In practice, the delay time τ should be chosen so that the elements of y_j are uncorrelated. If τ is too small, then the coordinates at x_j and $x_{j+\tau}$ represent almost the same information. If τ is too large, then x_j and $x_{j+\tau}$ represent distinctly unrelated components of the embedding space. If the embedding dimension d is too small, the trajectory may cross itself. The requirement of a

sufficiently large embedding dimension prevents such ambiguity and ensures that the reconstruction is differentiable and invertible [2]. But an excessively large embedding dimension may lead to excessive computation and corrupt data, since noise will dominate the additional dimensions of the embedding space where no dynamics is operating [26].

There are several methods that have been proposed to determine the suitable delay time and the embedding dimension [1, 5, 9, 25]. We use the criterion proposed by Abarbanel [1] to determine the delay time τ to be approximately $1/10 - 1/20$ of the time associated with the first local minimum of the autocorrelation function of the measurement data $\{x_j\}$. The autocorrelation function is defined as

$$R(\tau) = \frac{1}{N} \sum_{i=1}^N x_{i+\tau} x_i, \quad (4.2)$$

and is shown in Figure 4.2 for the chaotic two-well data.

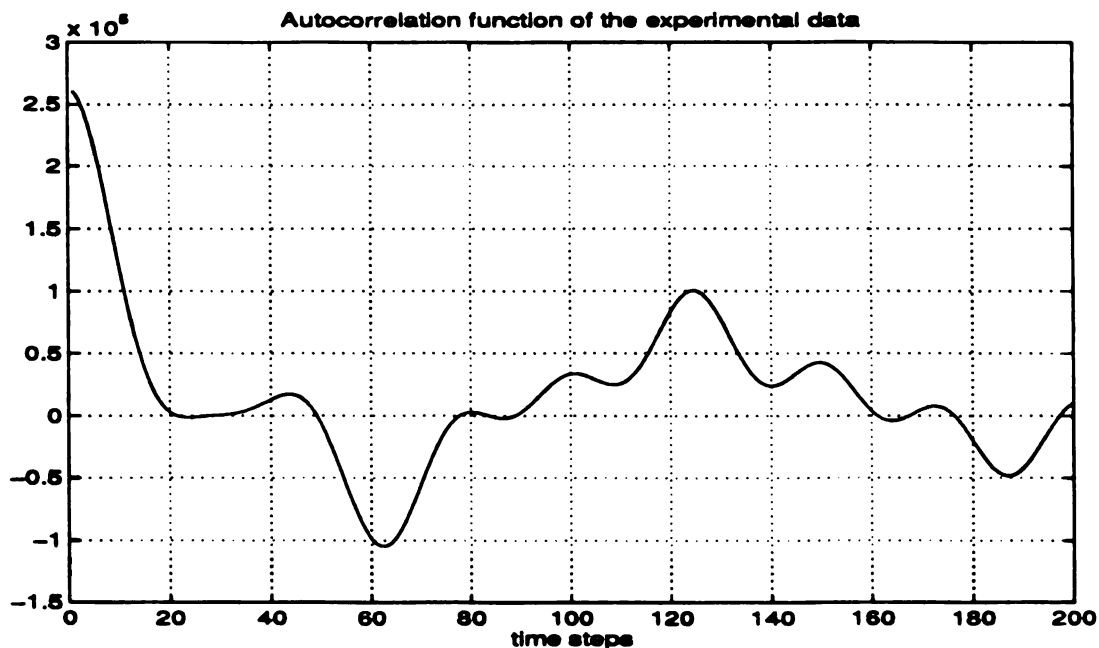


Figure 4.2 Autocorrelation function of the experimental data.

The prop

the sing

distribu

when

Eq. (

then

in t

[2,

de

ob

F

D

c

c

c

.

The proper embedding dimension is estimated by the correlation function method [27] and the singular system analysis method [9]. The correlation function method calculates the distribution of points within a small region for a large data set, such that

$$C(r) = \lim_{r \rightarrow 0} \frac{1}{N^2} \sum_i^N \sum_j^N H(r - |y_i - y_j|) \quad (4.3)$$

where $H(z)=1$ if z is positive; and $H(z)=0$ otherwise; y is a pseudo-vector constructed as Eq. (4.1). If the attractor is properly unfolded by choosing a sufficiently large dimension, then any property associated with the attractor which depends on distances between points in the phase space would become independent of the value of the embedding dimension [2, 15, 27]. In a regime that $C(r)$ becomes independent of d , and exhibits a power law dependence on r as $r \rightarrow 0$, that is $\lim_{r \rightarrow 0} C(r) = ar^d$, the correlation dimension could be

obtained by measuring the slope of the plot of $\log C(r)$ versus $\log r$, such as

$$d = \lim_{r \rightarrow 0} \frac{\log C(r)}{\log r} \quad (4.4)$$

Figure 4.3 shows the plot of $\log C(r)$ versus $\log(r)$ for several values of the dimension d . The slopes are about 2.5, which becomes independent of the dimension as $d \geq 3$. Ding *et al.* [15] reported that the plateau begins when the embedding dimension first exceeds the correlation dimension. Thus, this criterion should produce a lower bound to our required embedding dimension.

The singular-system analysis method involves constructing a covariance matrix $C = Y^T Y$ and decomposing it into two unitary matrices U and V and a diagonal matrix Σ , such that

logC(t)

where

Eq.

sing

sho

By

un

be

fo

A

fr

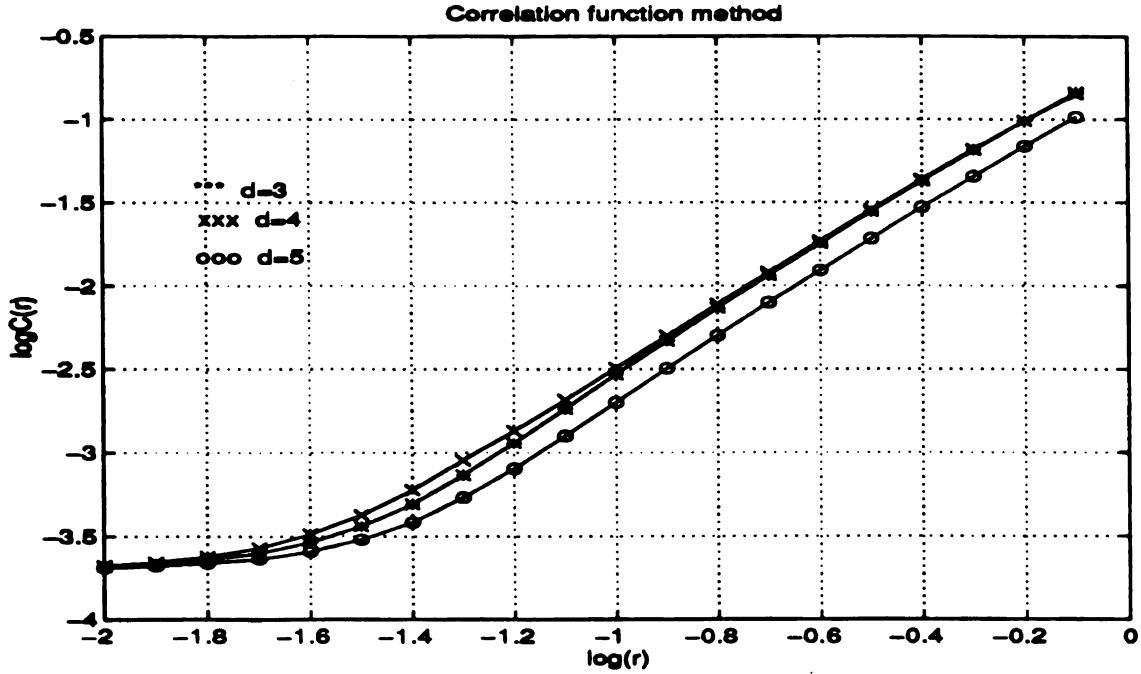


Figure 4.3 Correlation function of the experimental data.

$$C = U\Sigma V^T, \quad (4.5)$$

where Y is the matrix with each column containing the pseudo-vector y as constructed in Eq. (4.1). Varying the dimension in constructing the pseudo-vectors, and conducting the singular values analysis, a plot of the singular values versus the embedding dimension is shown in Figure 4.4.

By comparing the singular values with the values induced by 'noise', which is assumed uniformly distributed in the extra dimensions and will be nearly equal, the singular values become flat when $d \geq 4$. Thus we determine the suitable embedding dimensions to be four.

A two dimensional projection of the reconstructed phase space is shown in Figure 4.5, from which the unstable periodic orbits are to be extracted for use in our identification

singular values

algo

coor

4.4

Fro

des

wh

ex

sin

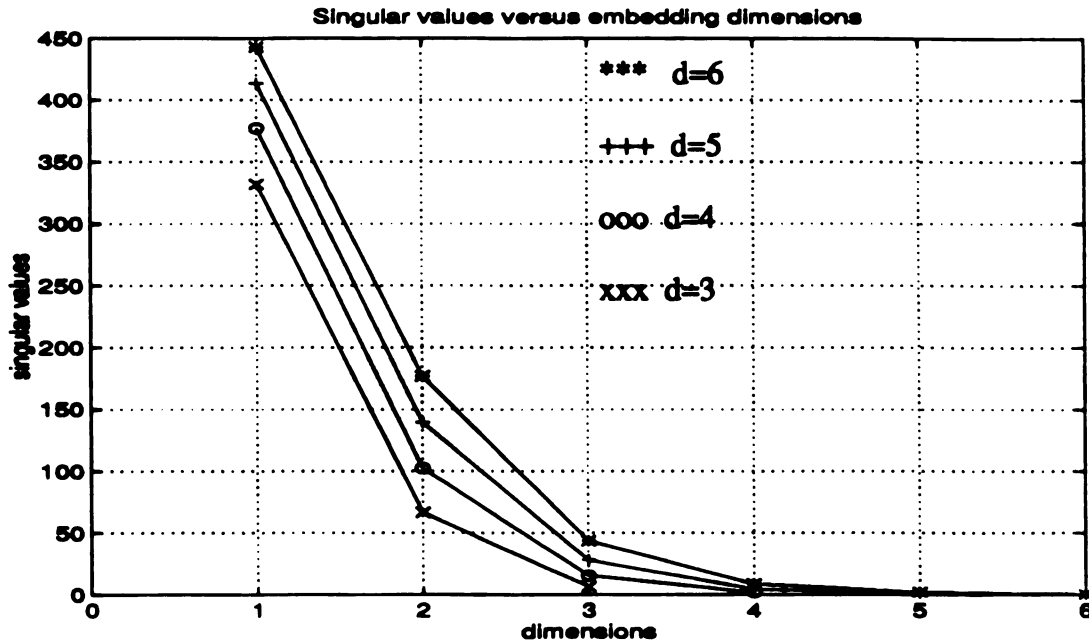


Figure 4.4 Singular system analysis of the experimental data.

algorithm. Also, a transformation of the reconstructed phase space into the singular coordinates is performed by using the singular vectors, as shown in Figure 4.6.

4.4 Periodic-Orbit Extraction

From the reconstructed chaotic attractor, the unstable periodic orbits can be extracted as described in Chapter two. In the pseudo phase space, we seek recurrent points such that

$$|y_{i+k} - y_i| \leq \epsilon \quad (4.6)$$

where ϵ is set as 0.5% of the maximum extent of the chaotic set as before. Some of the extracted periodic orbits are shown in Figure 4.7. The corresponding periodic orbits in the singular coordinate are shown in Figure 4.8.

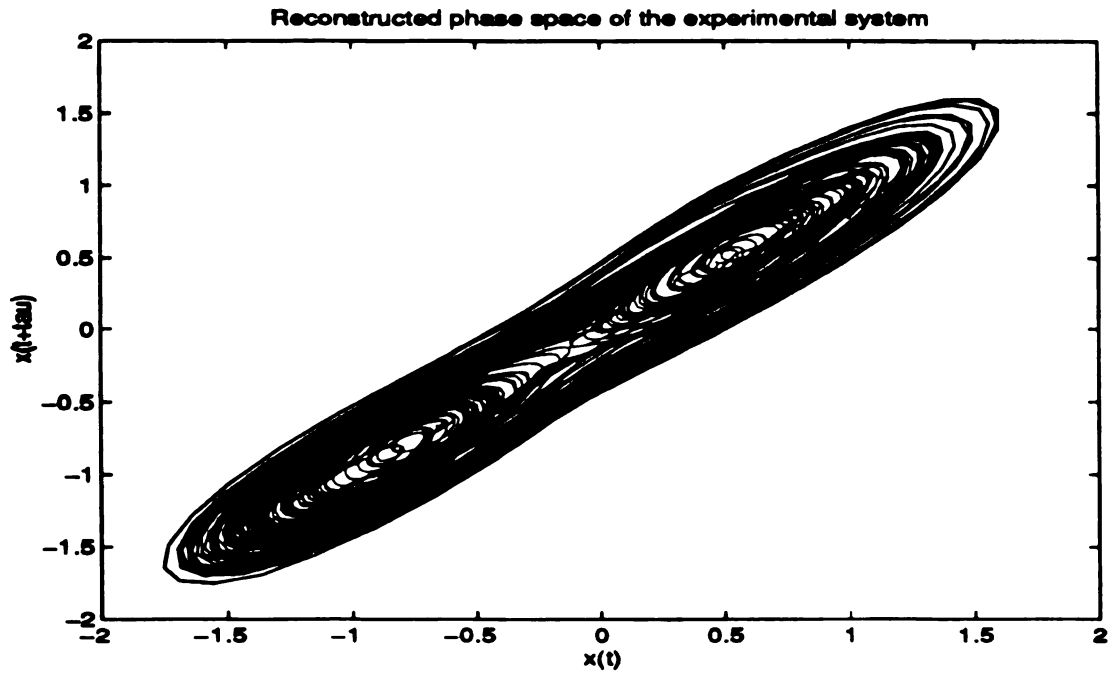


Figure 4.5 Reconstructed phase space of the experimental system

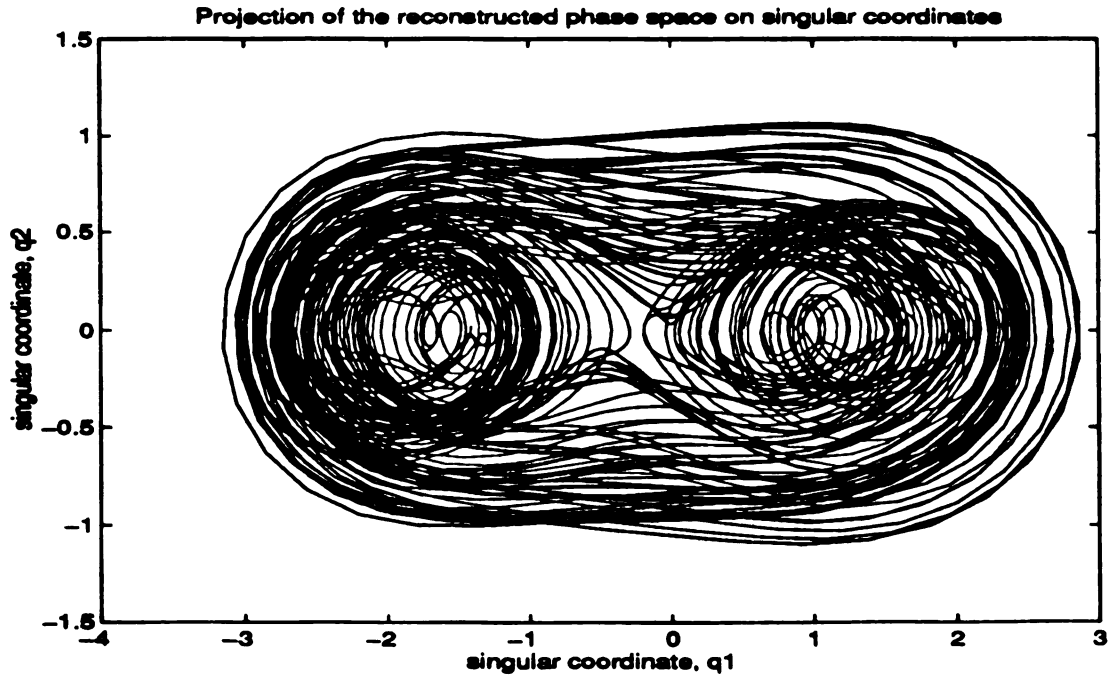


Figure 4.6 Reconstructed phase space in singular coordinates

2

1

$x(t+\tau)$

$x(t+\tau)$

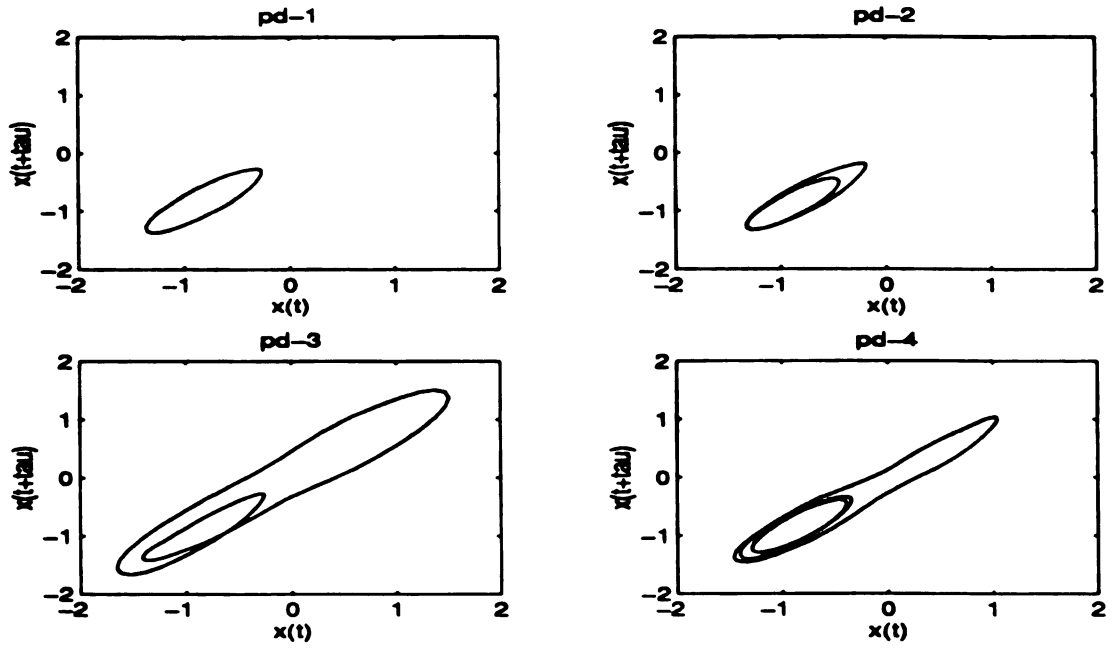


Figure 4.7 Some extracted periodic orbits from the reconstructed phase space

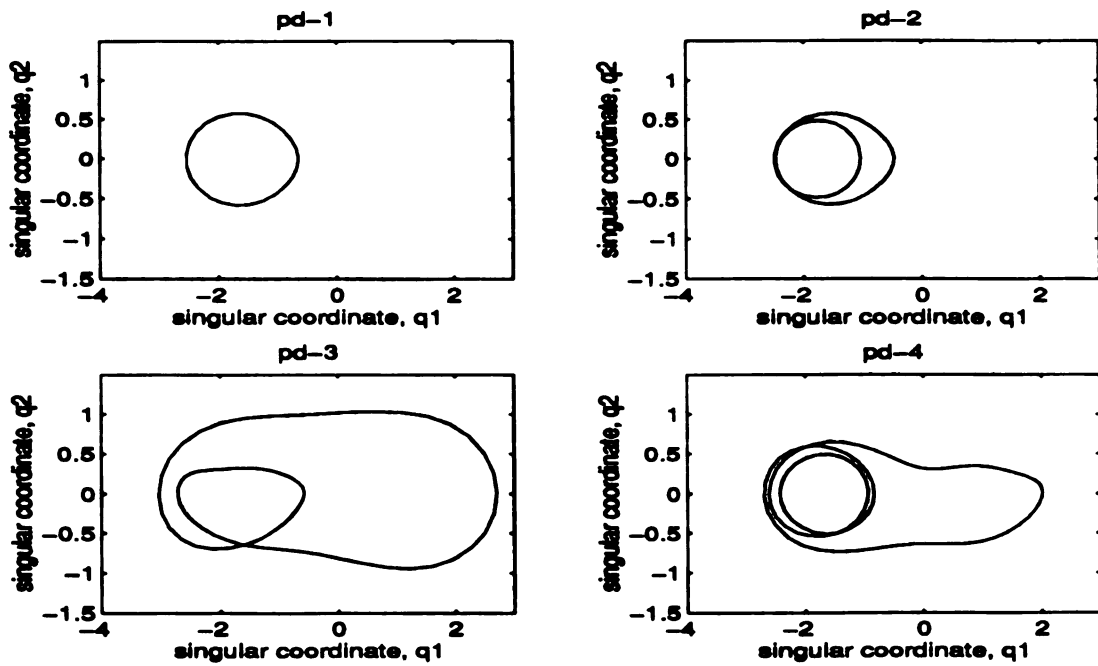


Figure 4.8 Some extracted periodic orbits in singular coordinates

4.5 Choosing a Mathematical Model

Knowing the experimental system is an externally excited nonlinear system with a two-well potential, we choose a mathematical model in a polynomial form to fit the characteristics of the nonlinear function. We choose a polynomial because we know that the magnetic and elastic forces are smooth. We do not know, however, whether a power series converges to the actual stiffness characteristic in the domain of displacement. Furthermore, in the case of divergence, we do not know the optimal truncation of the series representation. Our best hope is to obtain a model which qualitatively fits the characteristic of the experimental system.

The model with viscous damping is then written as

$$m\ddot{x} + \alpha\dot{x} + \sum_{i=1}^p \beta_i x^i = a \cos \omega t, \quad (4.7)$$

where m , α , and β_i are the parameters to be determined, p is the number of terms in the power series.

4.6 Data Processing Issues

The experimental data are in a digital format, ranging from -2048 to 2047 corresponding to -5V to 5V of the voltage output from the A/D converter. There is a scaling factor between the digital numbers and the actual physical unit. The parameters in Eq. (4.7) are scaled by this factor in a nonlinear fashion. Assume that the factor between the digital data z and the variable x in Eq. (4.7) is a constant γ in units of (displacement unit)/(digital unit), such that

$$x = \gamma z. \quad (4.8)$$

Substituting this into Eq. (4.7), the model equation can be rewritten as

$$(m\gamma) \ddot{z} + (\alpha\gamma) \dot{z} + \sum_{i=1}^P (\beta_i \gamma^i) z^i = a \cos \omega t. \quad (4.9)$$

Since the digital data are large in amplitude, the high-order nonlinear terms will be even larger in amplitude, causing an ill-conditioning of the matrix A used in the least-squares fit. To prevent this, we can choose γ in such a way as to normalize the data to the unit interval. The time variable can also be nondimensionalized to a new variable, $\tilde{t} = \omega t$. This normalization of time is manifested in the velocity and acceleration terms, and improves the conditioning of the least-squares problem.

Meanwhile, we know that the external forcing is periodic, although the forcing amplitude is unknown. This implies that Eq. (4.9) is actually indeterminate, and one of the quantities in the equation has to be taken as known and moved to the right hand side of the equation, as having been done in the parametrically excited and the autonomous cases in previous chapter.

In this work, we deal with the unknown forcing amplitude by discarding the first harmonic of Eq. (4.9) so that the other parameters may be identified. Another approach would be to include the forcing amplitude as unknown sine and cosine coefficients to be identified.

Hence, we divide through Eq. (4.9) by the quantity $m\gamma\omega^2$, and recast it in a form as

$$\tilde{\alpha} z' + \sum_{i=1}^P \tilde{\beta}_i z^i = z'' + \tilde{a} \cos \tilde{t}, \quad (4.10)$$

where $\bar{\alpha} = \alpha/m\omega$, $\bar{\beta}_i = \beta_i\gamma^{i-1}/m\omega^2$, and $\bar{a} = a/m\gamma\omega^2$, are the scaled parameters to be determined.

Using the extracted periodic orbits, each term in the model equation (4.10) is periodic and expressed in a Fourier series as done before. The Fourier coefficients of the multiples of primary harmonics, except the first harmonic, are balanced to form a set of algebraic equations in system parameters for least-squares estimations as usual. The phase angles associated with the extracted periodic orbits are ignored since the harmonics which balance the forcing function are not used.

4.7 Identification Results and Model Verification

Using ten extracted periodic orbits together in the identification algorithm, with the data being processed as discussed above, and using four terms in the polynomial in the model Eq. (4.9), i.e., $p=4$, identification results are shown in Table 14.

Table 14: Identification results for the experimental system

periodic orbits	$\bar{\alpha}$	$\bar{\beta}_1$	$\bar{\beta}_2$	$\bar{\beta}_3$	$\bar{\beta}_4$
1 to 10	0.034	-0.266	0.141	0.323	-0.041
6, 8, 10	0.025	-0.304	0.184	0.338	-0.078
3, 5, 7, 9	0.041	-0.269	0.190	0.346	-0.067
3 to 9	0.034	-0.244	0.199	0.338	-0.070
Average	0.035	-0.280	0.178	0.336	-0.064
Std. dev	0.007	0.041	0.026	0.0096	0.016

The ide

orbits.

corresp

factor

We ha

stiffn

nega

dam

eno

As

sm

lec

To

fu

av

W

te

g

o

in

W

Ho

The identification results are consistent by using different combinations of the periodic orbits. The standard deviation of each identified parameter is small compared to the corresponding average value. The values in the table are scaled to SI units by an unknown factor as discussed in previous section.

We have also used a third-degree polynomial in the identification process. The identified stiffness parameters were similar to those in Table 14. However, the damping term was negative. A priori knowledge tells us that the damping should be positive. Since the damping is small, it is likely that slight inadequacy in the third-degree model caused enough error in the damping term to reverse its sign.

As in Chapter three, we are tempted to neglect the 4th-degree term since its coefficient is small. However, we favor the identified parameters based on the 4th-degree model since it led to a reasonable damping term.

To show effect of the 4th-degree term in range of data, we first examine the nonlinear function of the system by plotting it with the identified parameter values. Using the average values in Table 14, the nonlinear function is shown in Figure 4.9.

Within the scaled data range, the curves are qualitatively similar using three and four terms in the power series. The curves represent a nonlinear function similar to the one generated by a two-well potential to which the experimental system belongs. Hence, we obtain a qualitative model for the experimental system, with unknown factors as discussed in previous section, Eq. (4.10), in the following equation:

$$z'' + 0.035z' - 0.28z + 0.178z^2 + 0.336z^3 - 0.064z^4 = \bar{a}\cos\bar{t}. \quad (4.11)$$

We proceed to do a numerical simulation using the identified model of Eq. (4.11). However, since the force amplitude is unknown, we estimate it indirectly. By substituting

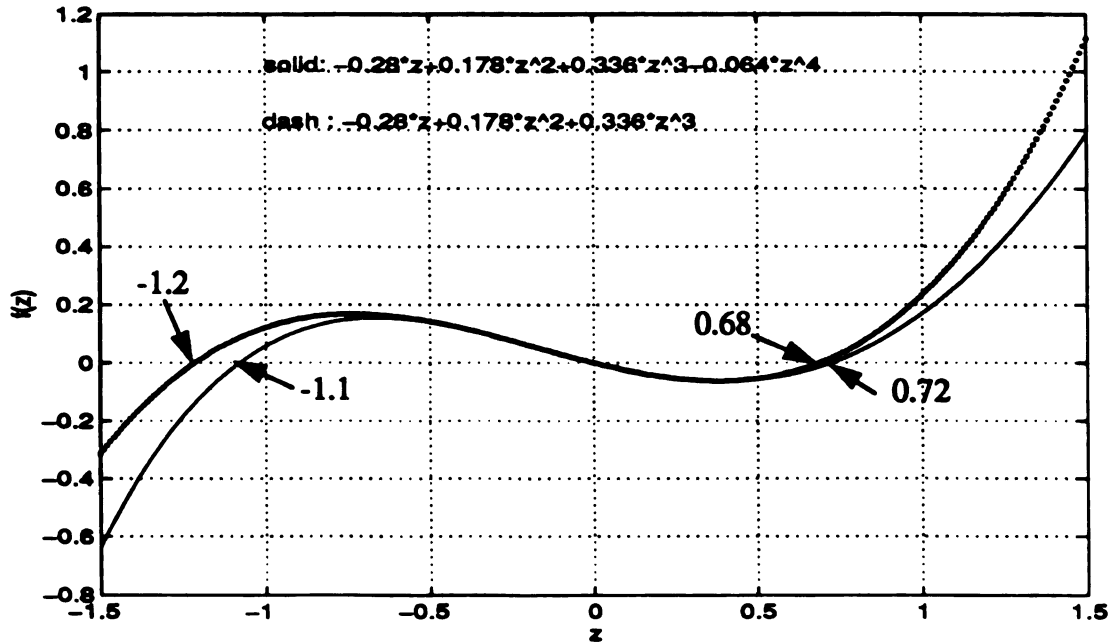


Figure 4.9 Qualitative nonlinear function of the experimental system.

the identified values into the algebraic equations $A\alpha = q$ formed from balancing the first harmonic, we find that the force amplitude \bar{a} to be 0.25 on average by using the first ten extracted periodic orbits.

We also conduct a bifurcation diagram using the identified model by slowly increasing the forcing amplitude as done experimentally, and sampling the steady-state response at the same time interval. We carry out two bifurcation diagrams, one with the nonlinearity up to the cubic term in the equation, the other one with the fourth term, as shown in Figure 4.10. Both parameter sets came from the same 4th-degree model. Figure 4.10(a) shows a nonperiodic response when the force amplitude is in the range of 0.23~0.29 for the model with cubic nonlinearity, and about 0.2~0.29 for the model with fourth power nonlinearity in Figure 4.10(b). In the forcing range shown in the diagrams, the bifurcation diagrams are

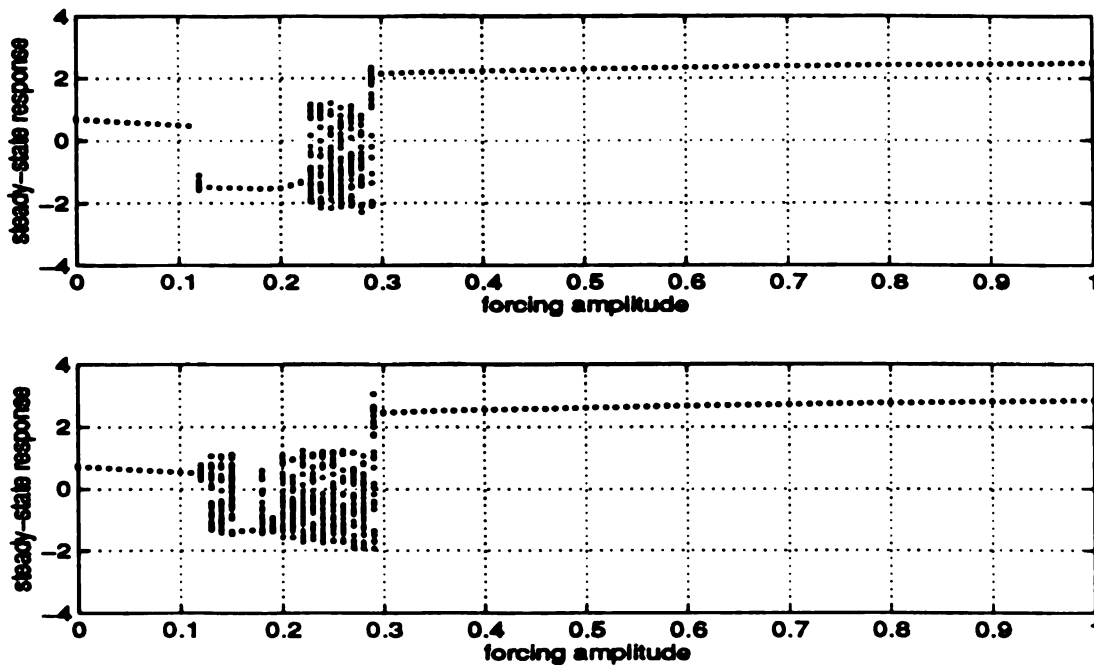


Figure 4.10 Bifurcation diagram of the identified model, (a) with the cubic nonlinear term in the model, and (b) with the fourth power term in the model

similar. As the forcing amplitude increases beyond four, the bifurcation diagrams are different, since the fourth nonlinear term makes the system globally unstable.

The calculated forcing amplitude can generate chaotic motion, as happened experimentally. Hence, a forcing amplitude $\bar{a} = 0.25$ is used as a typical one in Eq. (4.11) for numerical simulations.

Numerical integration of Eq. (4.11) is carried out using a Runge-Kutta method as usual. The phase portrait of the model with cubic nonlinearity is shown in Figure 4.11, from which the unstable periodic orbits are extracted as shown in Figure 4.12.

There is some resemblance between the periodic orbits extracted from the reconstructed attractor in Figure 4.12 and the identified one in Figure 4.8. A large difference between periodic orbits extracted from the experimental and the numerical models does not

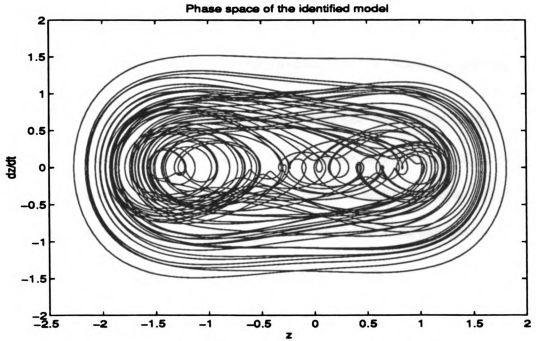


Figure 4.11 Phase portrait of the identified model with cubic nonlinearity

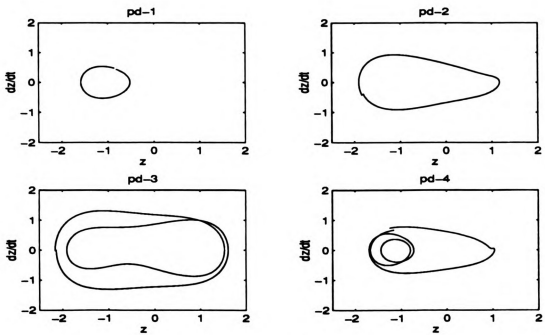


Figure 4.12 Some periodic orbits extracted from the phase portrait of Figure 4.11

exclude the possibility of the existence of more similar orbits. Thus, we can conclude that Eq. (4.11) qualitatively represents the experimental system. Given the mass and the scale factor γ discussed in section 4.6, the physical parameters can be obtained accordingly.

4.8 Estimation of the Natural Frequency and the Damping Ratio

Linearizing the identified model of Eq. (4.11) around the equilibrium points, we can calculate the eigenvalues of the linearized model, and hence estimate the natural frequencies and damping ratios for comparison with experimental measurements.

The Jacobian of Eq. (4.11) is

$$Df = \begin{bmatrix} 0 & 1 \\ -\beta_1 - 2\beta_2x - 3\beta_3x^2 + 4\beta_4x^3 & -\alpha \end{bmatrix} \quad (4.12)$$

The equilibrium points are obtained from Figure 4.9 by locating the zero-crossing of the nonlinear stiffness function. The equilibria for the curve with four nonlinear terms are 0.72 and -1.1. Then the eigenvalues of Eq. (4.12) are $-0.0175 \pm 0.6348i$ and $-0.0175 \pm 0.9426i$ in the time-normalized system. The real part represents the decaying rate, and the imaginary part represents the undamped natural frequency ω_n . The damping ratio can be calculated by dividing the real part by the imaginary part, yielding 2.76% and 1.86% for the right and the left well respectively. Converting to real time system by multiplying by the driving frequency (7.5 Hz in this case), the damped natural frequencies $\omega_d = \omega_n \sqrt{1 - \zeta^2}$ are 4.76 Hz and 7.07 Hz, respectively.

Omitting the fourth degree nonlinear term, the equilibrium points are 0.68 and -1.2 from Figure 4.9, and the eigenvalues of the linearized model are $-0.0175 \pm 0.6541i$ and

$-0.0175 \pm 0.8626i$. The damping ratio becomes 2.68% and 2.03%, and the real time damped natural frequencies are 4.91 Hz and 6.47 Hz for the right and the left well respectively

The transfer functions of the experimental system were measured by Bart Kimble¹, as shown in Figure 4.13.

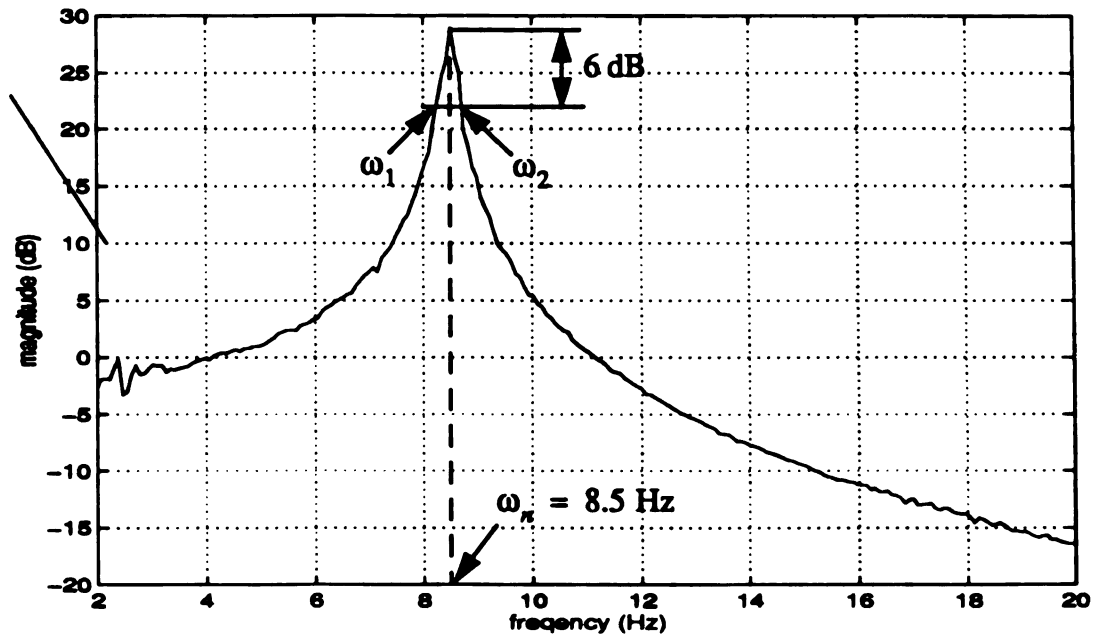


Figure 4.13 Transfer function of the right well of the experimental system

Using the half-power point method, and assuming the damping ratio, ζ , is small, the damping ratio can be estimated by

$$\zeta = \frac{\omega_2 - \omega_1}{2\omega_n} \quad (4.13)$$

1. The transfer functions of the experimental system were kindly given by Bart Kimble at Penn State University.

when

is the

con

the

(4

s

v

where ω_1 and ω_2 are the frequencies at the half-power point of the transfer function, ω_n is the undamped natural frequency, as indicated in Figure 4.13. Table 15 contains a comparison of the natural frequencies and the damping ratios of the linearized model and the experimental measurement. Since the stiffness function in the identified model, Eq. (4.11), is in some sense a best fit to the experimental stiffness function, variation in the slope of these functions leads to variations in linearized quantities.

Table 15: Comparison of the natural frequency and the damping ratio

wells	ω_d and ζ	experimental measurement	linearized model with cubic nonlinearity	linearized model with fourth nonlinearity
right well	ω_d	7.7 Hz	4.91 Hz	4.76 Hz
	ζ	2.73%	2.68%	2.76%
left well	ω_d	8.5 Hz	6.47 Hz	7.07 Hz
	ζ	2.52%	2.03%	1.86%

4.9 Discussion

Using the experimental data, we reconstructed the phase space of the experimental system, from which the unstable periodic orbits were extracted for use in our parametric identification algorithm. A qualitative model is obtained to represent the experimental system as Eq. (4.11).

There are some discrepancies in the identification results when using different extracted periodic orbits individually. We used several periodic orbits together because different

perio

prov

info

For

wh

periodic orbit visits different area of the reconstructed phase space. Using several of them provides a better representation of the system behavior, and also gives some statistical information of the identification results.

For this reason, chaotic dynamics is beneficial for parameter identification, particularly when the form of the model is approximate. We will revisit this issue in next chapter.

CHAPTER 5

Errors in Parameter Estimates

5.1 Introduction

Errors are inevitable in any parametric identification method, arising from the incorrect modelling, data acquisition and data manipulations. Modelling is not only a main source of error, but also a critical factor for the success of an identification method. We have discussed this issue when we presented our method in Chapter Two, and some criteria have been used to validate the model in Chapter Three.

In this chapter, we will focus on the quality of the data, and its effect on the formulation of the least-squares estimation $A\alpha = q$. An obvious source of error is the noise, which is inherent to the data acquisitions and manipulations. We will treat it as external to the system response, and assume it is random and bounded. We have also used the unstable periodic orbits exclusively in our identification scheme for a chaotic system. The unstable periodic orbits are extracted from a chaotic attractor, and used as an approximation of the real periodic orbit of the system. The deviation of the extracted unstable periodic orbits from the real one is another source of error to be discussed in detail.

5.2 Errors induced by Noise

Suppose some noise $n(t)$ is added to a periodic orbit $p(t)$, such that

$$\bar{p}(t) = p(t) + n(t), \quad (5.1)$$

where the noise is assumed to be uniformly distributed and uncorrelated to the periodic orbit. Applying this noisy periodic-orbit data to a power-series model (assumed to be valid), a nonlinear term x^k in the model is expressed in a Fourier series in a form

$$F\{(\bar{p})^k\} = F\{p^k + knp^{k-1} \dots\} = F\{p^k\} + kF\{np^{k-1}\} \dots, \quad (5.2)$$

where F denotes the Fourier series representation.

Suppose that the upper bounds of $p(t)$ and $n(t)$ are known, i.e., there exists real positive numbers \wp and ζ , such that

$$|p(t)| \leq \wp, \text{ and } |n(t)| \leq \zeta, \quad (5.3)$$

for $t \in [0, T]$. The Fourier coefficients of the real periodic orbit are

$$\begin{aligned} a_{jk} &= \frac{2}{T} \int_0^T p^k(t) \cos(j\omega t) dt \\ b_{jk} &= \frac{2}{T} \int_0^T p^k(t) \sin(j\omega t) dt \end{aligned} \quad (5.4)$$

where the subscript k refers to the nonlinear term x^k .

Similarly, the Fourier coefficients of the noise-contaminated periodic orbit can be calculated as

$$\begin{aligned} \bar{a}_{jk} &= \frac{2}{T} \int_0^T \bar{p}^k(t) \cos(j\omega t) dt \\ \bar{b}_{jk} &= \frac{2}{T} \int_0^T \bar{p}^k(t) \sin(j\omega t) dt \end{aligned} \quad (5.5)$$

Thus, the differences of the Fourier coefficients between $\bar{p}^k(t)$ and $p^k(t)$ will be bounded by the following relationship:

$$\begin{aligned} |\Delta a_{jk}| &\equiv |a_{jk} - \bar{a}_{jk}| = \frac{2}{T} \left| \int_0^T (p^k(t) - \bar{p}^k(t)) \cos(j\omega t) dt \right| \\ &= \frac{2}{T} \left| \int_0^T \left(\sum_{i=1}^k \frac{k!}{(k-i)!i!} p^{k-i}(t) n^i(t) \right) \cos(j\omega t) dt \right| \\ &\leq 2 \sum_{i=1}^k \frac{k!}{(k-i)!i!} \varphi^k \left(\frac{\zeta}{\varphi} \right)^i \end{aligned} \quad (5.6)$$

for every harmonic j . Normalizing the error bound of Eq. (5.6) by φ^k yields

$$\frac{|\Delta a_{jk}|}{\varphi^k} \leq 2k \left(\frac{\zeta}{\varphi} \right) + k(k-1) \left(\frac{\zeta}{\varphi} \right)^2 + \dots \quad (5.7)$$

The arguments will be the same for $|\Delta b_{jk}| = |b_{jk} - \bar{b}_{jk}|$.

For $k = 1$, the bound depends on the bound of noise only, which is usually assumed to be as small as a few percent, specified by the noise-to-signal ratio, ζ/φ . As k increases, the error bound will accumulate, making the perturbations in A larger accordingly. If the degree of the nonlinear term in the mathematical model is excessively large, the accuracy of the estimation results will deteriorate rapidly by the noise.

Having these bounds on $|\Delta a_{jk}|$ and $|\Delta b_{jk}|$, we can determine a bound on $\|\Delta A\|$ and $\|\Delta q\|$ due to noise¹. Then by a method given in section 5.4 below, a bound on the error of the identified parameters, $\|\Delta \alpha\|$, can be estimated.

1. All norms here are Euclidean 2-norms.

5

A

h

th

c

w

P

P

C

P

5.3 Errors Induced by the Periodic Orbit Extraction

Another source of errors comes from the extraction of the unstable periodic orbits. We have specified a spatial criterion ε in the state space, such that $\|x_{i+k} - x_i\| \leq \varepsilon$, to look for the recurrent points in a large chaotic data set. We presume that when the trajectory comes close to a periodic orbit, it approximately follows the motion of that periodic orbit, so that when the recurrent points are located, the segment of data is taken as the approximate periodic orbit. This approximation is related to a characteristic quantity of the associated periodic orbit as discussed below.

Consider a neighborhood $\mathcal{N}(\bar{x})$ of a saddle fixed point \bar{x} of a period- k orbit in the Poincare section, as sketched in Figure 5.1.

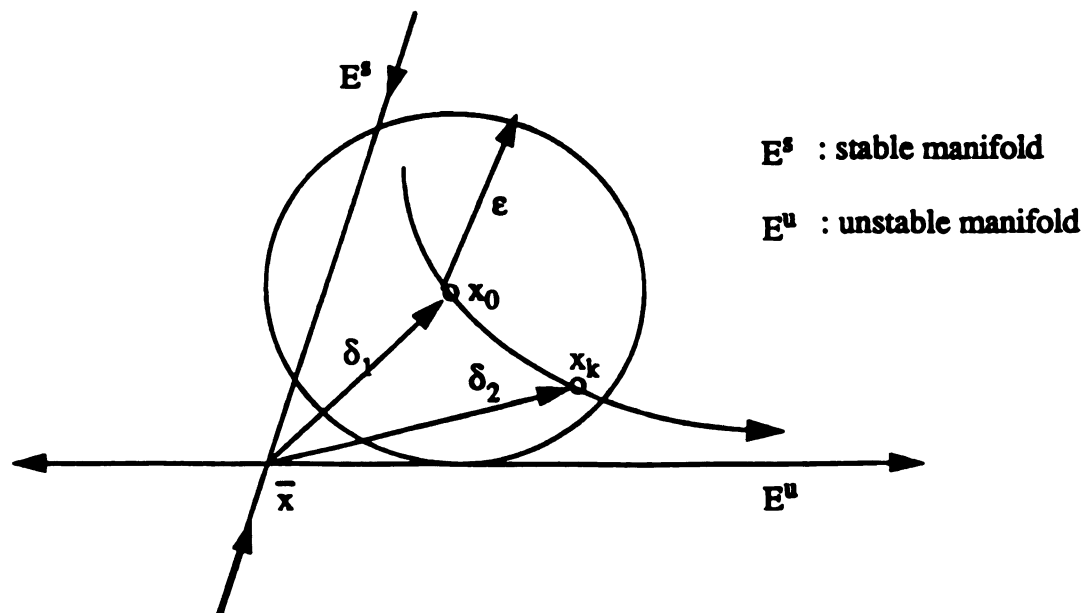


Figure 5.1 Close look of the periodic orbit extraction on the Poincare section

The dynamics of the system in this neighborhood can be viewed in terms of a linear map T , such that

$$x_{n+k} - \bar{x} \approx T(x_n - \bar{x}) \quad (5.8)$$

where T is the linearized map about the period- k orbit \bar{x} in the period- k Poincare section, which is invertible, since the periodic point is a saddle for a chaotic system, and \bar{x} is the saddle point, representing the true periodic orbit of a nonlinear system. If the orbit is near the saddle to be considered as an approximate periodic orbit of period k , then by the linearized map, the spatial distance between an orbit and its k iterations can be written as

$$\begin{aligned} \|x_k - x_0\| &= \|(x_k - \bar{x}) - (x_0 - \bar{x})\| \\ &= \|T(x_0 - \bar{x}) - (x_0 - \bar{x})\| \\ &= \|(T - I)(x_0 - \bar{x})\| \leq \varepsilon \end{aligned} \quad (5.9)$$

Taking the matrix norm, Eq. (5.9) is bounded by the singular values of the matrix $(T - I)$, such that

$$\lambda_2 \|x_0 - \bar{x}\| \leq \|(T - I)(x_0 - \bar{x})\| \leq \lambda_1 \|x_0 - \bar{x}\|, \quad (5.10)$$

where λ_1 and λ_2 are the maximum and the minimum singular values of the matrix $(T - I)$. Since $\|(T - I)(x_0 - \bar{x})\| \leq \varepsilon$, the distance between the approximate periodic orbit and the true periodic orbit, by the criterion $\|x_k - x_0\| \leq \varepsilon$, is bounded by

$$\delta_1 \equiv \|x_0 - \bar{x}\| \leq \varepsilon / \lambda_2. \quad (5.11)$$

Note that, since \bar{x} is a saddle point, the singular value λ_2 will not be zero in any case.

Similarly, taking the map backward, the spatial distance becomes

$$\|x_k - x_0\| = \|(x_k - \bar{x}) - T^{-1}(x_k - \bar{x})\| = \|(T^{-1} - I)(x_k - \bar{x})\|, \quad (5.12)$$

and the distance between x_k and the saddle is bounded by

$$\delta_2 \equiv \|x_k - \bar{x}\| \leq \varepsilon / \mu_2, \quad (5.13)$$

where μ_2 is the smallest singular value of the matrix $(T^{-1} - I)$, which is non-zero because \bar{x} is a saddle point. Thus the approximate periodic orbit by the criterion of $\|x_k - x_0\| \leq \varepsilon$ will be bounded by the larger of δ_1 and δ_2 , i.e.

$$\delta = \max\{\delta_1, \delta_2\} \leq \max\left\{\frac{\varepsilon}{\lambda_2}, \frac{\varepsilon}{\mu_2}\right\}. \quad (5.14)$$

Since λ_2 and μ_2 are the minimum singular values of matrices relating to the linearized map of the periodic orbit, the bound δ in Eq. (5.14) bounds the error of the extracted periodic orbit. The smaller the pre-specified spatial criterion ε is, the smaller the bound δ will be. However, the criterion ε should be determined by the data set, since excessively small ε may result in no data points fitting in the criterion.

With the error bound δ determined by the characteristic of the periodic orbit as above, we can proceed to bound the errors in A and q , i.e. we can find a bound on $\|\Delta A\|$ and $\|\Delta q\|$ due to the periodic-orbit extraction. The argument is the same as that presented in previous section, Eq. (5.2) to (5.6), except that the upper bound of noise ζ is replaced by the error bound δ .

In reality, we have to analyze the data to approximate the map T . The procedure follows ideas of [5,18, 19,35,49].

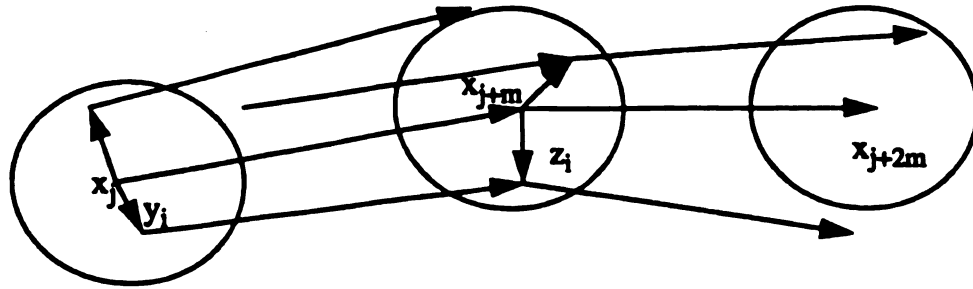


Figure 5.2 A sketch of the construction of a linearized map

Let $\{x_j\}$, $j = 1, \dots, P$, be a set of data points in state space, denoting a periodic orbit extracted from a chaotic attractor¹. We intend to find a sequence of local linearized maps T_j , $j = 1, \dots, M$, by increments of m , such that

$$x_{j+m} = T_j x_j \quad (5.15)$$

where $M = P/m$, an integer, and $x_{(M+1)m} = x_m$, since the orbit is periodic. Then we construct a compound map by multiplying each local linearized map T_j in a reverse order, such as

$$T = T_M T_{M-1} \dots T_1 \quad (5.16)$$

This compound map T represents the total linearized map of the periodic orbit, as the one used in Eq. (5.8) on the period- k Poincare section. Figure 5.2 is a sketch of the construction of this linearized map.

1. It should be noted that we used the same notation x for points on the Poincare section earlier in this section.



Consider a small ball of radius r centered at the orbital point x_j , and a set of n data points $\{x_{k_i}\}$, $i = 1, \dots, n$, included in the ball. The number of data points n is to be discussed later. The set of displacement vectors between x_{k_i} and x_j is formed as

$$\{y_i\} = \{x_{k_i} - x_j \mid \|x_{k_i} - x_j\| \leq r\} . \quad (5.17)$$

After the evolution of a time interval $\tau = m\Delta t$, the orbital point x_j will proceed to x_{j+m} and the neighboring points x_{k_i} to x_{k_i+m} . The displacement vectors y_i are thereby mapped to

$$\{z_i\} = \{x_{k_i+m} - x_{j+m} \mid \|x_{k_i} - x_j\| \leq r\} . \quad (5.18)$$

The evolution time interval $m\Delta t$ effects the quality of the linearization, depending on the dynamics of the system. If $m\Delta t$ is too small, the map will resemble an identity map. If $m\Delta t$ is too large, nearby points evolve beyond the regime of linearity. We have found no proposed method for optimizing the choice of m . Usually we choose m to be one or two.

Let Y be a matrix containing the vectors y_i and Z containing the vectors z_i . If the radius r is small enough, evolution of Y to Z can be approximated by a linear mapping represented by a matrix T_j , such that

$$Z \cong T_j Y . \quad (5.19)$$

By minimizing the squared error norm of Eq. (5.19) with respect to all components of the matrix T_j , we obtain an expression for T_j as

$$T_j = \left(Y Y' \right)^{-1} \left(Z Y' \right), \quad (5.20)$$

where $(.)'$ denotes the matrix transpose. The matrix T_j is an approximation of the linearized map at x_j . If there is no degeneracy, Eq. (5.20) can be solved for T_j . In some situations, Y may not be uniformly distributed in all direction of x_j (because of the data), and may not span the entire phase space, such that $\left(Y Y' \right)^{-1}$ does not exist and the matrix T_j may not be well defined. In such case, we might simply skip it and proceed to the next point x_{j+m} , or use larger ball to find another set of neighboring points to eliminate the degeneracy. In this way, we can construct a sequence of linearized maps for the periodic orbits, and multiply each one around the periodic orbit in reverse order as that in Eq.(5.16) to obtain the final map for use in Eq. (5.11) and (5.13).

To include enough neighboring points, n , around the orbital point for constructing the linearized map, the radius of the neighborhood has to be larger than the spatial criterion used to find the approximate periodic orbit. Lathop and Kostelich [35] used a radius of 6ϵ to include 50 or more points. Eckmann and co-workers [5,18,19] increased the radius until 30 or more points were found, while Sano and Sawada [49] set the number of points to be 20, and confirmed that lower number still gave similar results, provided that number was greater than the embedding dimension.

5.4 Sensitivity of the Parameter Estimates to Errors

Knowing the error bounds $\|\Delta A\|$ and $\|\Delta q\|$ induced by the noise and by the periodic orbit extraction, we could proceed to estimate the sensitivity of the parameter estimation results

to these errors.

Let ΔA and Δq be the perturbations of A and q respectively in the linear system, with A being a full-rank matrix. Define

$$\begin{aligned}\alpha &= A^\dagger q \\ \alpha^* &= (A + \Delta A)^\dagger (q + \Delta q), \\ r &= q - A\alpha\end{aligned}\tag{5.21}$$

where A^\dagger is the *pseudo-inverse* of A , which yields the optimal least-squares solution of $A\alpha = q$, as does the $(A + \Delta A)^\dagger$ for α^* in Eq. (5.21). Assuming

$$\eta \equiv \max\left[\frac{\|\Delta A\|}{\|A\|}, \frac{\|\Delta q\|_2}{\|q\|_2}\right] < \frac{1}{\text{cond}(A)},\tag{5.22}$$

and

$$\sin(\theta) \equiv \frac{\|r\|_2}{\|q\|_2} < 1,\tag{5.23}$$

implicitly defining θ , $0 \leq \theta < \pi/2$, then the error in the parameters α is bounded by [4]

$$\frac{\|\alpha^* - \alpha\|_2}{\|\alpha\|_2} \leq \eta \left[\frac{2\text{cond}(A)}{\cos\theta} + \tan\theta [\text{cond}(A)]^2 \right] + O(\eta^2).\tag{5.24}$$

For a given model and given periodic orbits, A and q are fixed, and η is determined by $\|\Delta A\|$ and $\|\Delta q\|$ induced by the error sources discussed in previous sections. If the model is chosen properly, the residual, r , is usually very small, resulting in small θ . Thus the error bound is Eq. (5.24) depends linearly on $\text{cond}(A)$. If the model is not properly chosen, the error bound is Eq. (5.24) will depend on the square of $\text{cond}(A)$, making the error bound sufficiently larger. From numerical results presented in Chapter Three, we found that the

choice of a model is the most influential factor on estimating the parameters. Also, an improperly chosen model results in a large condition number for A , resulting in a violation of the assumption in Eq. (5.22). In fact, this occurred when we tried to compute the bound of the error in section 3.1.5. In that example, we directly computed $\|\Delta A\|$ and $\|\Delta q\|$ by comparing the quantities in the noise-free and noisy cases. Thus, the estimate (5.23) may not always be practical, but at least indicates some trends.

5.5 Using Several Periodic Orbits

In this section, we discuss how an application of several periodic orbits together in the identification scheme, as opposed to using a single periodic orbit, can reduce the sensitivity of the parameter estimates to errors.

Suppose a mathematical model has been chosen, and different matrices A_i are formed using p different periodic orbits, such that $i = 1, \dots, p$. Suppose different sets of parameters $\hat{\alpha}_i$ are then estimated from

$$A_i \hat{\alpha}_i = q_i, \quad i = 1, \dots, p. \quad (5.25)$$

Then, combining several A_i into a single matrix A , such that

$$A^T = [A_1^T, A_2^T, \dots, A_p^T], \quad (5.26)$$

and combining the corresponding q_i into a single vector q , we obtain a set of parameters

$\hat{\alpha}$ from the combined equation, $A\hat{\alpha} = q$, through

$$(A^T A)\hat{\alpha} = A^T q, \quad (5.27)$$

which is equivalent to

$$\left(\sum_{j=1}^P A_j^T A_j \right) \hat{\alpha} = \sum_{j=1}^P A_j^T q_j \quad (5.28)$$

Summing Eq. (5.25) on i , and subtracting from Eq. (5.28), yields

$$\sum_{j=1}^P A_j^T A_j (\hat{\alpha} - \hat{\alpha}_j) = \sum_{j=1}^P A_j^T A_j \left((\hat{\alpha} - \alpha) + (\alpha - \hat{\alpha}_j) \right) = 0, \quad (5.29)$$

where α is the true parameter vector. Defining

$$\begin{aligned} R_i &= \left(A^T A \right)^{-1} \left(A_i^T A_i \right) \\ \Delta &= \alpha - \hat{\alpha} \\ \Delta_i &= \alpha - \hat{\alpha}_i \end{aligned} \quad (5.30)$$

we obtain an expression of the error using different sets of periodic orbits, as

$$\Delta = \sum_{j=1}^P R_j \Delta_j \quad (5.31)$$

Note that, $\sum_{j=1}^P R_j = I$. Thus, Eq. (5.31) implies that the error in parameter estimates from

several periodic orbits is a weighted average of parameter errors from individual periodic orbits, through the weights R_j . If a particular periodic orbit were known to yield the best estimation, we would use it for identification. However, we have no idea which one will be the best in general. Hence, using a combination of several periodic orbits has advantages. It can give a reasonable estimate, reduce the sensitivity to errors, and improve the statistical properties of the identified results, which has been shown in our previous applications.

CHAPTER 6

Conclusions and Future Work

6.1 Conclusions

We have presented a method for identifying parameters of nonlinear systems that exhibit chaotic behaviors. This is an extension of an existing method for nonlinear systems with stable periodic response. We exploit the chaotic attractor of the nonlinear system by extracting the unstable periodic orbits from the chaotic attractor to represent the system behavior. Each term in the mathematical model is expressed in a finite Fourier series using the extracted periodic orbit, and the harmonic-balance method is applied to form a set of linear algebraic equations in system parameters for least-squares estimation. We have demonstrated that the present approach is applicable to externally excited, parametrically excited, and autonomous chaotic systems. This may not be feasible using other methods.

Although chaos has been regarded as undesirable noise to be discarded from the physical systems, it has rich information content as compared to a periodic trajectory. This richness has been exploited in dimensionality studies, nonlinear prediction, and control. The central theme is the presence of unstable periodic orbits, which can be extracted and used to characterize the chaotic attractor. Therefore they are useful in parametric identification for a chaotic system. Furthermore, the availability of many periodic orbits with different

periods provides a 'persistent excitation' for a system with many parameters. This is an advantage of using chaos in parametric identification.

Modelling is an important issue in the parametric identification scheme. The model must be able to catch the essential characteristics of the system under investigation, such as the form of the nonlinearity and the type of excitation. For smooth systems throughout this study, we choose a power series to represent the system nonlinearity, based on the fact that a smooth function can be expressed in a power series around the equilibrium points. Some questions related to this representation, such as how to choose the optimal truncation of the power series, and whether or not the data are within the radius of convergence of the series, remain to be studied further. We have discussed this problem using a numerical example in Chapter Two. We found that, when the data are within the radius of convergence of the power series, the model can be accurately identified. When the data are out of the radius of convergence, the accuracy of identification results deteriorate. In such case, the real nonlinear function of the system has to be known in order to obtain accurate results. Knowing something about the system under investigation is fundamental for parametric identification. Otherwise, we have to be content with partial description of the identified system. The moral is that good models lead to good quantitative results.

We have applied this method numerically to several chaotic systems, such as a forced Duffing oscillator, a smooth Coulomb friction oscillator, a parametrically excited beam, and a Lorenz oscillator. The accuracy is typically within 1% error of the identified parameters for noise-free data. When the noise level increases, the accuracy deteriorates, although in a robust way, especially when the mathematical model is not properly chosen.

We have also applied this method to a forced mechanical oscillator with a two-well

stiffness potential. Chaotic data were acquired from a strain gauge by an analog-to-digital converter. The data were proportional to the displacement of the oscillator. The amplitude of the periodic forcing function was unknown. We modeled the experimental system in a power series. The unstable periodic orbits were extracted from a reconstructed attractor using the method of delays. Consistency of the identified parameters was achieved using different combinations of the extracted periodic orbits, leading to a qualitative description of the system nonlinearity, and hence to a qualitative model of the experimental system. A bifurcation diagram was constructed using the identified model, revealing phenomena of period doubling and chaos. This qualitative model can be useful for further investigation of the experimental system.

Models were verified by comparing the Lyapunov exponents, bifurcation diagrams, and the structure of the unstable periodic orbits in the original and the identified systems. We also sought consistency in the identified parameters by using different sets of periodic orbits.

Two main sources of errors in the parameter estimates, noise and the extraction of the unstable periodic orbits, have been examined closely from statistical and geometrical points of view. We considered the noise to be uncorrelated to the system response and uniformly distributed. We constructed a linearized map for the periodic orbits, and derived a bound by the singular values of the corresponding linearized map. By expressing the noisy periodic orbits in Fourier series, the error in the Fourier coefficients of a nonlinear term in the mathematical model can be bounded as a function of the noise-to-signal ratio. Errors enter the algebraic equations in a nonlinear fashion, increasing the uncertainty of the identification results. The error bound of the parameter estimates is proportional to the

square of the conditional number of the matrix A of the identification equations, $A\alpha = q$, if the residuals are large. Otherwise, the error bound is linear in $\text{cond}(A)$. We found that using several extracted periodic orbits together will reduce the sensitivity of the parameter estimates to these errors.

6.2 Future Work

We have used the unstable periodic orbits exclusively to represent the system behavior in our parametric identification scheme. The system is in a form of an ordinary differential equation, and recast as a set of linear algebraic equations through the balancing of the Fourier coefficients of each term in the equation. This is strategically convenient for our applications, but not mathematically rigorous. Further studies may lead to a better understanding of how it relates to the ordinary differential equation.

We expressed the periodic orbit in a Fourier series, using the fundamental frequency in calculating their Fourier coefficients. The Fourier series of a period N orbit consists of frequency components m/N , $m = 1, \dots, N$, thus making available many harmonics to balance. It may be worth examining whether subharmonics or superharmonics yield better results.

Errors in the identification process can be investigated more thoroughly by examining how they manifest themselves in the formulation of the least-squares estimation, such as the extraction of the unstable orbits from the chaotic attracting set and the fluctuation of the Fourier coefficients of these unstable periodic orbits.

We chose to use polynomials as the basis functions to model the system nonlinearity. Other form of basis functions such as wavelets, Pade functions, sigmoid functions, and radial functions, might be worth investigation.

Experimental work can be explored further, such as with autonomous systems and higher degree-of-freedom systems. Quantitative studies, involving specific material or system parameters, such as in identifying the elastic modulus, might be valuable. Experimental studies on distributed systems would complement the numerical work of Yasuda and co-workers [59, 60, 61], and might raise other interesting issues.

This study focused on smooth nonlinear functions. Non-smooth systems, such as impact and friction, might call for adjustments in this method.

Also, adapting this method to identify parameters which are expressed nonlinearly in the differential equation of motion, such as in arguments of functions (e.g. $\tanh(\alpha x)$) requires some development. An extension of the present method to broadband spectra, by balancing the real and imaginary parts of the Fourier transform of each term, may accommodate the case of noisy input.

BIBLIOGRAPHY

BIBLIOGRAPHY

- [1] Abarbanel, H. D. I., Brown, R., and Kadtke, J. B., "Prediction in Chaotic Nonlinear Systems: Methods for time series with Broadband Fourier Spectra", *Physical Review A*, 41, 1990, 1782-1807
- [2] Abarbanel, H. D. I., Brown, R., and Tsimring, L. S. "The Analysis of Observed Chaotic Data in Physical Systems", *Reviews of Modern Physics* 65, 1993, 1331-1392
- [3] Aguirre, L. A. and Billings, S. A., "Validating Identified Nonlinear Models with Chaotic Dynamics", *International J. Bifurcation and Chaos*, Vol. 4, 1994, 109-125
- [4] Atkinson, K. E., *An Introduction to Numerical Analysis*, 2nd ed., John Wiley and Sons, 1989
- [5] Auerbach, D., Cvitanovic, P., Eckmann, J. P., Gunaratne, G., and Procaccia, I., "Exploring chaotic motion through periodic orbits", *Physical Review Letter*, 58, 1987, 2387-2389
- [6] Beck, J. and Arnold, K., *Parameter Identification in Engineering and Science*, John Wiley & Sons, 1977
- [7] Breeden, J. L., and Hubler, A., "Reconstructing Equations of Motion from Experimental Data with Hidden Variables", Technical Report CCSR-90-7, University of Illinois at Urbana-Champaign, 1990
- [8] Bridge, J. and Rand, R., "Chaos and Symbol Sequence in System with a Periodically Disappearing Figure-Eight Separatrix," *Bifurcation Phenomena and Chaos in Thermal Convection*, ASME HTD-Vol.214/AMD-Vol.138, 1992, 47-55
- [9] Broomhead, D. S., and King, G. P., "Extracting Qualitative Dynamics from Experimental Data", *Physica D* 20, 1986, 217-236
- [10] Coppola, V. T., and Rand, R. H., "Chaos in a System with a Parametrically Disappearing Separatrix," *Nonlinear Dynamics* 1, 1990, 401-420
- [11] Crutchfield, J. P. and McBamara, B. S., "Equations of Motion from a Data Series," *Complex System* 1, 1991, 417-452
- [12] Cusumano, J. P. and B. W. Kimble, "Experimental Observation of Basins of Attraction and Homoclinic Bifurcation in a Magneto-Mechanical Oscillator," in *Nonlinearity and Chaos in Engineering Dynamics*, edited by J. M. T. Thompson and S. R. Bishop, John Wiley & Sons Ltd, 1994

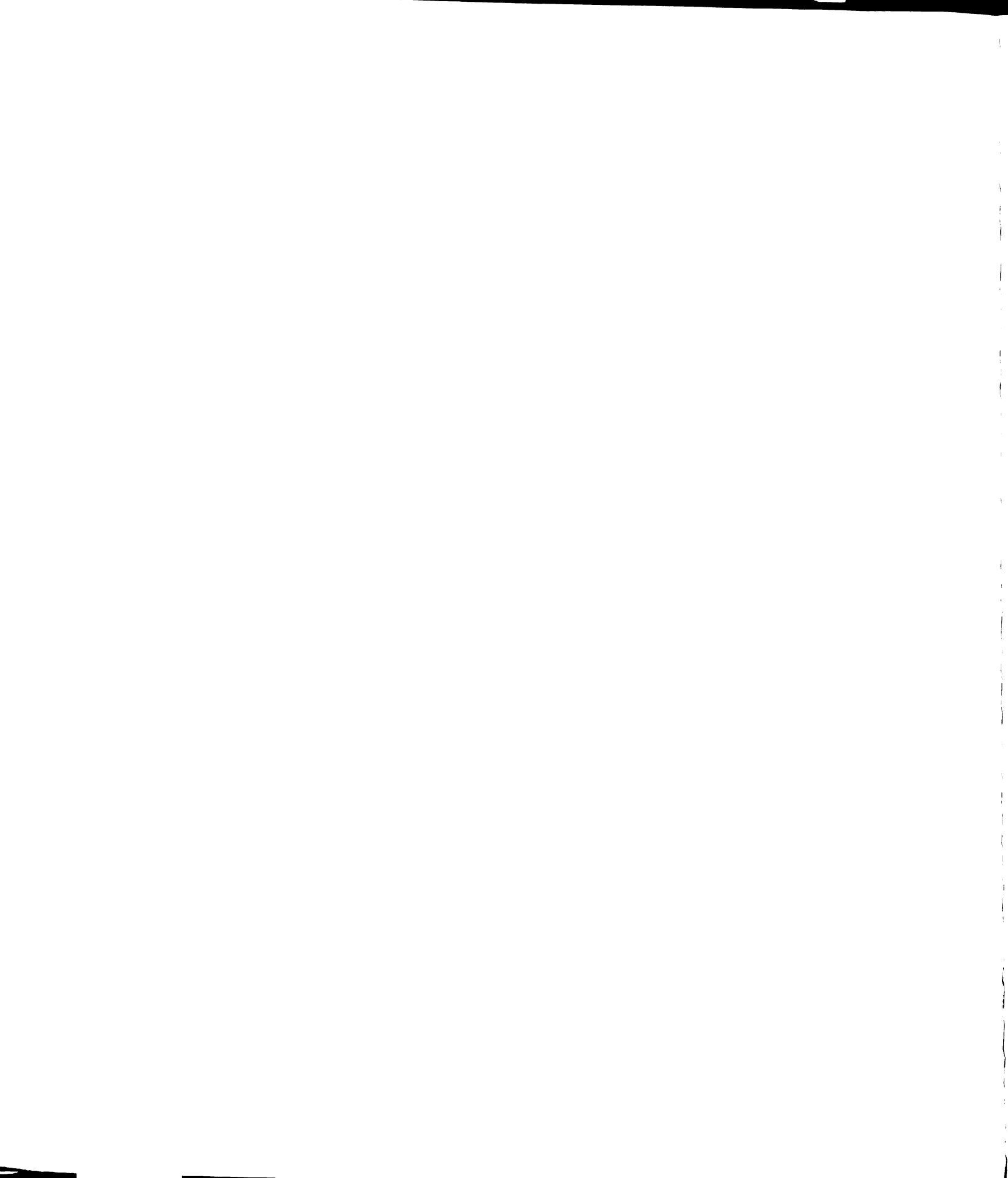
- [13] Cusumano, J. P., and Sharkady, M. T., "An Experimental Study of Bifurcation, Chaos, and Dimensionality in a System Forced Through a Bifurcation Parameter" To appear
- [14] Cvitanovic, P, Gunaratne, G. H., and Procaccia, I., "Topological and metric properties of Henon-type strange attractor," *Physical Review A*, 38, 1988, 1503-1507
- [15] Ding, M., Grebogi, C., Ott, E., Sauer, T., and Yorke, J. A., "Plateau Onset for Correlation Dimension: When Does It Occur?", *Physical Review Letters*, 70, 1993, 3872-3875
- [16] Ditto, W. L., Rauseo, S. N., and Spano, M. L., "Experimental Control of Chaos", *Physical Review Letter*, 65, 1990, 3211-3214
- [17] Distefano, N., and Rath, A., "System identification in nonlinear structural seismic dynamics", *Comput. Mech. Appl. Mech. Engng* 5, 1975, 353-372
- [18] Eckmann, J.-P., "Ergodic theory of chaos and strange attractors", *Reviews of Modern Physics*. 57, 1985, 617-656
- [19] Eckmann, J.-P., Kamphorst, S. O., Ruelle, D. and Ciliberto, S., "Lyapunov Exponents from Time Series", *Physical Reviews A*, 34, 1986, 4971-4979
- [20] Eisenhammer, T., Hubler, A., Packard, N., and Kelso, J. A. S., "Modeling Experimental Time Series with Ordinary Differential Equations", Technical Report CCSR-89-7, University of Illinois at Urbana-Champaign, 1989
- [21] Farmer, J. D. and Sidorowich, J. J., "Predicting Chaotic Time Series", *Physical Review Letters*, 59, 1987, 845-848
- [22] Feeny, B. F. and Liang, J-W, "Phase-space reconstruction of stick-slip systems", submitted to the 15th Biennial ASME conference on Noise and Vibration, 1995
- [23] Feeny, B. F., Nayfeh, A. H., and Mook, D. T., "Parametric identification via the method of multiple scales: modeling a ship at sea", to appear
- [24] Feeny, B. F., and Moon, F. C., "Chaos in a Forced Dry-Friction Oscillator: Experiments and Numerical Modelling", *J. Sound and Vibration*, 170, 1994, 303-323
- [25] Fraser, A. M., and Swinney, H. L., "Independent Coordinates for Strange Attractors from Mutual Information", *Physical Review A*, 33, 1986, 1134-1140
- [26] Gershenfeld, N., "An Experimentalist's Introduction to the Observation of Dynamical Systems", in *Directions in Chaos*, Vol. 2, edited by Hao B.-L., World Scientific, N. J., 1988
- [27] Gottlieb, O., Feldman, M., and Yim, S. C. S., "Parametric Identification of Nonlinear

Ocean Mooring Systems Using the Hilbert Transform”, preprint

- [28] Grassberger, P. and Procaccia, I., “Characterization of Strange Attractors”, *Physical Review Letter*, 50, 1983, 346-349
- [29] Grebogi, C., Hammel, S. M., Yorke, J. A., and Sauer, T., “Shadowing of Physical Trajectories in Chaotic Dynamics: Containment and Refinement,” *Physical Review Letters*, 65, 1990, 1527-1530
- [30] Guckenheimer, J., Holmes, P., *Nonlinear Oscillations, Dynamical Systems, and Bifurcations of Vector Fields*, Springer-Verlag New York, 1983
- [31] Hammel, S. and Heagy, J., “Chaotic System Identification Using Linked Periodic Orbits”, *SIAM Conference on Applications of Dynamical Systems*, Snowbird, Utah, 1992.
- [32] Hanagud, S. V., Meyyappa, M., and Craig, J. I., “Method of Multiple Scales and Identification of Nonlinear Structural Dynamic Systems” *AIAA Journal*, Vol. 23, May 1985, 353-372
- [33] Ibanez, P., “Identification of Dynamic Parameters of Linear and Nonlinear Structural Models from Experimental Data,” *Nuclear Engineering and Design*, 25, 1973, 30-41
- [34] Kennel, M. B., Brown, R., and Abarbanel, H. D. I., “Determining Embedding Dimension for Phase Space Reconstruction Using a Geometrical Construction”, *Physical Review A*, 45, 1992, 3403-3411
- [35] Kesaraju, R. V., and Noah, S. T., “Characterization and Detection of Parameter Variations of Nonlinear Mechanical Systems”, *Nonlinear Dynamics* 6, 1994, 433-457
- [36] Lathrop, D. P. and Kostelich, E. J., “Characterization of an experimental strange attractor by periodic orbits”, *Physical Review A* 40, 1989, 4028-4031
- [37] Ljung, L., *System Identification--Theory for the User*, Prentice-Hall, 1987
- [38] Malasoma, J-M., Lamarque, C.-H., and Jezequel, L., “Chaotic Behavior of a Parametrically Excited Nonlinear Mechanical System,” *Nonlinear Dynamics* 5, 1994, 153-160
- [39] Mickens, R. E., “Bounds on the Fourier Coefficients for the Periodic Solutions of Nonlinear Oscillator Equations”, *J. Sound and Vibration*, 124, 1988, 199-203
- [40] Mohammad, K. S., Worden, K., and Tomlinson, G. R., “Direct parameter Estimation for Linear and Non-linear Structures”, *J. Sound and Vibration*, 152, 1992, 471-499
- [41] Mook, D. J. and Junkins, J. L., “Minimum Model Error Estimation for Poorly Modeled Dynamic Systems” *Journal of Guidance*, Vol. 11, No. 3, 1988, 256-261

- [42] Mook, D. J., "Estimation and Identification of Nonlinear Dynamic Systems" *AIAA Journal*, Vol. 27, July 1989, 968-974
- [43] Moon, F. C., *Chaotic and Fractal Dynamics--An Introduction for Applied Scientists and Engineers*, John Wiley and Sons, New York, 1992.
- [44] Moon, F. C. and Holmes, P., "A Magnetoelastic Strange Attractor," *J. Sound and Vibration*, 65, 1979, 275-296
- [45] Nayfeh, A. H., "Parametric Identification of Nonlinear Dynamic Systems", *Computer and Structures* Vol. 20, No. 1-3, 1985, 487-493
- [46] Nayfeh, A. H. and Mook, D. T., *Nonlinear Oscillations*, 1979
- [47] Ott, E., Grebogi, C., and Yorke, J. A., "Controlling Chaos", *Physical Review Letters*, 64, 1990, 1196-1199
- [48] Packard, N. H., Crutchfield, J. P., Farmer, J. D. and Shaw, R. S., "Geometry from a Time Series", *Physical Review Letters*, 45, 1980, 712
- [49] Sano, M., and Sawada, Y., "Measurement of the Lyapunov Spectrum from a Chaotic Time Series", *Physical Review Letters*, 55, 1985, 1082-1085
- [50] Shinbrot, T., Ott, E., Grebogi, C., and Yorke, J. A., "Using Chaos to Direct Trajectories to Targets", *Physical Review Letters*, 65, 1990, 3215-3218
- [51] Strang, G., *Linear Algebra and Its Applications*, 1976
- [52] Stry, G. I. and Mook, D. J., "An Experimental Study of Nonlinear Dynamic System Identification" *Nonlinear Dynamics*, 3, 1992, 1-11
- [53] Takens, F., in *Dynamic System and Turbulence, Warwick 1980*, edited by D. Rand and L.-S. Young, *Lecture Notes in Mathematics* No. 898 (Springer, Berlin, 1981)
- [54] Tufillaro, N. B., Abbott, T., and Reilly, J., *An Experimental Approach to Nonlinear Dynamics and Chaos*, Addison-Wesley Publishing Co, 1992
- [55] Ueda, Y., "Randomly Transitional Phenomenon in the System Governed by Duffing's Equation," *J. Statistical Physics* 20, 1979, 181-196
- [56] Ueda, Y., *The Road to Chaos*, Aerial Press, 1994
- [57] Wigdorowitz, B. and Petrick, M. H., "Modelling Concepts Arising from an Investigation into a Chaotic system," *Math. Comput. Modelling* 15, 1991, 1-16
- [58] Wolf, A., Swift, J. B., Swinney, H. L., and Vasano, J. A., "Determining Lyapunov Exponents from a Time Series," *Physica* 16D, 1985, 285-317

- [59] Yasuda, K., Kawamura, S., and Watanabe, K., "Identification of Nonlinear Multi-Degree-of-Freedom Systems (Presentation of an Identification Technique)", *JSME International Journal, Series III, Vol. 31, 1988, 8-14*
- [60] Yasuda, K., Kawamura, S., and Watanabe, K., "Identification of Nonlinear Multi-Degree-of-Freedom Systems (Identification Under Noisy Measurements)", *JSME International Journal, Series III, Vol. 31, 1988, 302-309*
- [61] Yasuda, K., and Kamiya, K., "Identification of a Beam (Proposition of an Identification Technique)", *JSME International Journal, Series III, Vol. 33, 1990, 535-540*



MICHIGAN STATE UNIV. LIBRARIES



31293014172708